Feasibility of Liquid Water Path Estimation of Over Land Using Satellite-Based Ka-Band Passive Microwave Data

Rie Seto, *Member, IEEE*, Toshio Koike, and Misako Kachi

***Abstract*— We investigate the feasibility of a method of estimating liquid water path (LWP, the sum of LWPs of cloud and rain) over land using satellite-based Ka-band passive microwave measurements. Specifically, we utilize brightness temperatures at 36.5 GHz (TB36) from the Advanced Microwave Scanning Radiometer for the Earth Observing System (AMSR-E). TB36 is appropriate for liquid-only estimation as it is less affected by ice scattering compared to higher frequency measurements. However, estimating LWP over land using TB36 is challenging due to weak cloud signals and strong and heterogeneous land radiation in TB36. To address this, our method (Le36) dynamically estimates land emissivity using lower frequency (6.9 and 10.7 GHz) measurements from AMSR-E, minimizing land radiation errors. Synthetic simulations indicated that Le36 has high performance in cases of a wide range of LWPs (∼8 kg/m^2) for cloud-only cases and a range of about 1.5∼8.0 kg/m^2 for cloud-plus-rain cases if the cloud top (CT) height is appropriately set. For cases without suitable CT settings, emphasis should be placed on high-CT clouds (>8000 m). In real-case applications, Le36 estimates showed reasonable agreement with independent cloud radar products, even over land. Furthermore, a comparison between Le36 and a method using 89.0 GHz (Le89) reveals that Le36 outperforms Le89 for liquid-only estimation, while estimates from Le89 include ice scattering effects. This study highlights the promising performance of Ka-band LWP estimation over land by mitigating the ice scattering effect and suggests the potential for more detailed cloud water content estimation using the TB36-TB89 difference.**

***Index Terms*— Dynamic land emissivity, Ka-band, liquid water path (LWP) estimation over land, satellite-based passive microwave remote sensing.**

I. Introduction

CLOUD and precipitation systems are composed of numerous hydrometeors, which are classified based on phase and particle size into categories such as liquid cloud, ice cloud, liquid precipitation (rain), and ice precipitation particles. The characteristics of a cloud and precipitation system—including the extent to which it develops and persists, whether it causes precipitation, and how strong such precipitation may be—are determined by the total amount and spatial distribution of water within the cloud system and the distribution of that water content among hydrometeor types within the cloud system [1], [2].

Because the features of rainfall carried by a cloud system can vary depending on the distribution of water particle types within the cloud system, even with the same total water content, the amounts of water in each type of hydrometeor are essential variables that constitute initial conditions for rainfall prediction. Furthermore, such variables are vital for the comprehension of cloud and precipitation processes, as well as the evaluation of rainfall prediction models. Thus, accurate observation data concerning the amounts of cloud water in each type of hydrometeor are desirable.

Currently, satellite-based remote sensing is widely used to estimate the vertically integrated liquid water content of cloud and precipitation systems [liquid water path (LWP)] because of its superior temporal coverage, spatial coverage, and data homogeneity. LWP can be empirically estimated from optical depth retrieved from infrared observation; however, this method can be applied to only the case of thin clouds (LWP∼0.1 kg/m^2) [3]. For the estimation of clouds with a wide range of LWP including large values (nearly several kilograms per square meter), there is a need to utilize microwaves that have the ability to penetrate large cloud systems, such as cumulonimbus systems. Thus, many studies have developed estimation algorithms that use satellite microwave measurements (e.g., [4], [5], [6]).

However, accurate estimation of water content in cloud and precipitation systems remains particularly challenging [7], [8]. Initially, clouds over land are generally excluded from satellite-based LWP estimation because the large spatiotemporal variations and uncertainties in land radiation obstruct the accurate estimation of LWP over land [9]. Accordingly, various LWP-related products, including the standard products of satellite radiometers, such as the Special Sensor Microwave Imager/Sounder, the Advanced Microwave Scanning Radiometer 2 (AMSR2), and the Advanced Microwave Scanning Radiometer-EOS [10], [11], [12], [13], [14], are available only over the ocean. The lack of LWP data over the Earth's entire land surface is a critical challenge in monitoring LWP, improving initial conditions, and evaluating models for rainfall predictions. Thus, a method for LWP estimation over land is urgently needed.

A few studies [15], [16] have estimated LWP over land using satellite-based microwave measurements, which involve high-frequency (approximately 90 GHz) microwaves,

Manuscript received 10 April 2023; revised 18 July 2023 and 5 October 2023; accepted 27 November 2023. Date of publication 7 December 2023; date of current version 26 December 2023. This work was supported by the Japan Aerospace Exploration Agency (JAXA) Research Announcement on the Earth Observations EO-RA3 under Grant ER3AMF218; and in part by the Grants-in-Aid for Scientific Research of Japan Society for the Promotion of Science (JSPS KAKENHI) under Grant JP20K14834 and Grant JP21K18744. *(Corresponding author: Rie Seto.)*

Rie Seto is with the Meteorological Research Institute, Tsukuba 305-0052, Japan (e-mail: rseto@mri-jma.go.jp).

Toshio Koike is with the International Centre for Water Hazard and Risk Management, Tsukuba 305-8516, Japan (e-mail: koike@icharm.org).

Misako Kachi is with the Japan Aerospace Exploration Agency, Tsukuba 305-8505, Japan (e-mail: kachi.misako@jaxa.jp).

Digital Object Identifier 10.1109/TGRS.2023.3340264

including relatively strong signals from hydrometeors within a cloud system. However, LWP estimation at these frequencies contains nonnegligible errors related to the scattering effect of ice particles [15]. This scattering effect is the second factor that contributes to high difficulty in LWP estimation. Seto et al. [16] designed a method for the estimation of LWP over land using satellite-based passive microwave brightness temperatures of 6.925, 10.65, 23.8, and 89.0 GHz (TB6, TB10, TB23, and TB89), with simultaneous estimation of land and atmospheric states (e.g., soil moisture, LWP, water vapor, and air temperature) based on optimization techniques (hereafter, this method is called Le89). The method successfully obtained reasonable LWP retrievals over land at several-kilometer resolution by dynamically representing land emissivity based on the soil moisture distribution that had been optimized by simultaneous satellite measurements. Nevertheless, those authors estimated LWP using TB89 assuming only liquid cloud water; they generated hydrometeors in other classifications (rain, ice cloud, and ice precipitation) using an atmospheric model that was implemented after estimation and assimilation. Thus, their method also included errors in LWP estimation related to the large effects of ice scattering.

In contrast, Ka-band microwave measurements are not substantially affected by ice scattering. Thus, for liquid-only estimation of water content within clouds, Ka-band microwaves are more appropriate. However, microwaves at these frequencies contain smaller cloud signals than microwaves at 89.0 GHz; accordingly, it is much more difficult to estimate LWP using Ka-band microwave measurements without higher frequency measurements (i.e., approximately 89.0 GHz), particularly over land.

With this background, the aim of this study is to examine the feasibility of a method for estimation of LWP over land using satellite-based passive microwave brightness temperatures at 36.5 GHz (TB36), which is included in the Ka-band, without temperatures at higher frequencies (e.g., 89.0 GHz). By using TB36 and removing the ice scattering effect, we develop a more accurate LWP estimation method over land.

In the following, we first confirm the basic characteristics of interactions between microwaves and hydrometeors through theoretical and simulation-related considerations to develop the idea of LWP estimation over land using TB36 and then examine possible strategies for LWP estimation with minimal effects related to ice scattering over land. Based on the strategies, we developed a new method for estimating LWP over land with TB36 (hereafter, this estimation method is called Le36). Then, we determine the scope of applications and the limitations of Le36 by conducting synthetic simulations and a sensitivity study. Finally, we evaluate the performance of Le36 by applying it to real cases of thick clouds and precipitation, and then comparing the estimation results of Le89 and Le36 with estimates from independent satellite cloud radar products. Based on these evaluations, we discuss the feasibility of LWP estimation over land with TB36, along with future challenges and perspectives.

II. Basic Concept of LWP Estimation Over Land Using Satellite-Based Microwave Measurements

In this section, we first describe the basic idea of LWP estimation over land using satellite-based passive microwave measurements, on which the Le36 and Le89 methods are based. We also describe the features of interactions between microwaves and hydrometeors through theoretical and simulation-related considerations, with a focus on surface type and polarization dependence. Based on these features, we examine the methodology for estimating LWP over land.

A. Simultaneous Estimation of Land State and LWP Using Satellite-Based Passive Microwave Measurements

Microwaves observed using satellites contain signals of the Earth's surface and atmosphere, including cloud particles. Emissivity in the microwave region and its heterogeneity are generally much higher for the land surface than for the ocean. This difference makes an accurate representation of land radiation and accurate LWP estimation much more difficult over land than over the ocean.

Materials that strongly affect microwave radiation can be remotely sensed using microwaves; the sensitivity of interactions between microwaves and materials depends on their wavelengths. Low-frequency microwave radiation (several to ten of gigahertz) does not extensively interact with the atmosphere or hydrometeors; thus, it is suitable for the estimation of land conditions with minimal influence from the atmosphere. Microwave radiation at approximately 23 GHz is generally absorbed well by water vapor and affected by hydrometeors, whereas interactions with hydrometeors become apparent at frequencies above ∼30 GHz [17].

Based on these characteristics, LWP estimation over land utilizes the frequency dependence of interactions of microwaves with hydrometeors and land states as follows. Initially, the land state is optimized through the estimation of soil moisture using low-frequency microwaves (6.925 and 10.65 GHz). From the optimized land state, land radiation at higher frequencies (23.8, 36.5, and/or 89.0 GHz) is physically calculated using a radiative transfer model (RTM) of land to provide background information for satellite-based LWP estimation. Then, LWP over land is estimated from measurements at a water vapor-sensitive frequency (23.8 GHz) and cloud-sensitive frequencies (89.0 or 36.5 GHz), which are obtained concurrently with low-frequency microwave data. In this methodology, we do not directly use the emissivity at lower frequencies, nor do we rely on statistical values, such as climate value, of emissivity. Instead, these procedures provide dynamic land emissivity, enabling the estimation of LWP with high accuracy even over heterogeneous land surfaces by simultaneous estimations of land and atmosphere.

B. Interactions Between Hydrometeors and Microwaves

Interactions between microwaves and hydrometeors are determined by their electromagnetic characteristics and the sizes of hydrometeors relative to microwave wavelengths. Hydrometeors emit and absorb microwaves depending on their temperature and water content, and they scatter microwaves depending on their size and shape.

Most cloud particles are smaller than ∼0.01 mm in diameter. Thus, for interactions between cloud water particles and microwaves at most wavelengths, the Rayleigh scattering approximation can be applied. Because the imaginary component of the complex refractive index of liquid water is

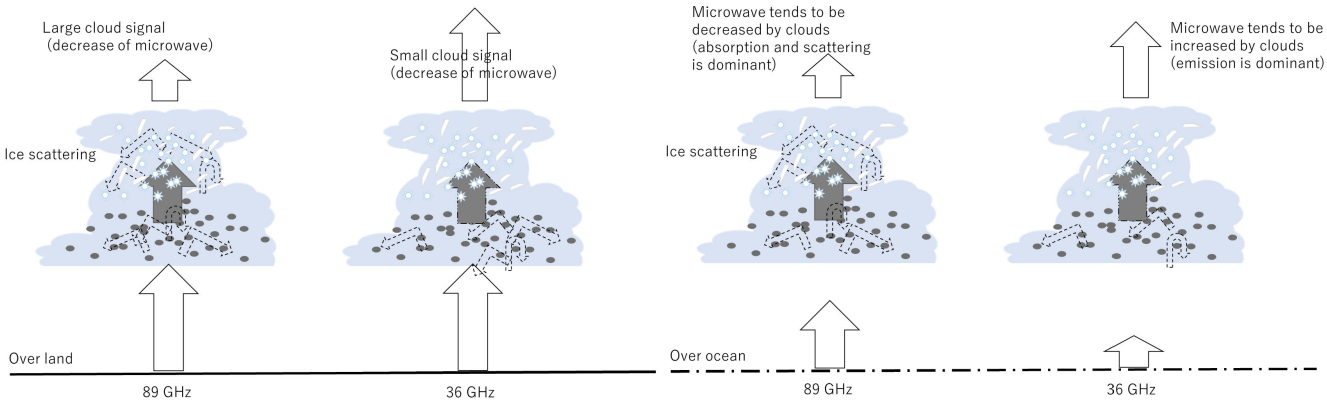

Fig. 1. Schematic of differences in interactions between hydrometeors and microwaves at 36.5 and 89.0 GHz over (left) land and (right) ocean. Over the ocean, the surface radiation is much weaker compared to land at 36.5 GHz. The emission by hydrometeors predominates over absorption and scattering of weak radiation from the ocean surface. Microwaves over land tend to decrease through a cloud layer regardless of frequency because of strong radiation from the land surface.

large, the effects of absorption and emission by liquid cloud particles are much greater than the effect of scattering in the Rayleigh region. For interactions between microwaves and large-diameter precipitation particles, the Rayleigh scattering approximation becomes inappropriate; the scattering effect must be considered in addition to absorption and emission. For solid water (ice), the imaginary component of the complex refractive index is small. Therefore, the scattering effect of ice particles is dominant compared with the absorption effect for the microwave region.

The intensity of interactions (absorption, emission, and scattering) also depends on the wavelength of the microwave radiation. The extinction of microwaves by ice particles is smaller than the extinction by liquid particles at low frequencies; however, it increases at high frequencies. Thus, cloud ice particles do not strongly affect low-frequency microwaves.

Radiation in the microwave region near 89 GHz is strongly attenuated by hydrometeors. Thus, satellite measurements at this frequency include relatively large signals from clouds and are applicable to the estimation of cloud water content (CWC) over land [15], [16]. Instead, such signals are largely affected by ice scattering [18]. Previous studies (e.g., [19]) have shown that brightness temperatures near 85 GHz can be strongly depressed in the presence of large ice particles. Therefore, estimates of LWP (liquid-only cloud water) based on high-frequency microwaves near these frequencies (including Le89) may contain errors related to the presence of mixed signals from hydrometeors in different categories.

At approximately 36.5 GHz, the wavelengths of microwave radiation (∼8 mm) are longer than the wavelengths of 89.0-GHz microwaves (∼3 mm). According to the size parameter, the Rayleigh approximation can be applied to the interaction between ice cloud particles and microwaves at 36.5 GHz. The scattering by ice cloud particles influences net radiation, but its impact is much smaller at 36.5 GHz than at 89.0 GHz [6], [17]. Thus, for LWP estimation, it is appropriate to use the brightness temperature at 36.5 GHz (TB36) because microwaves at this wavelength are less affected by ice water. However, the magnitude of the hydrometeor signal is much less in TB36 than in TB89 such that a more precise estimation algorithm is necessary for accurate LWP estimation when TB36 is used than when TB89 is used.

The attenuation by rain particles is expected to affect TB36, but the attenuation coefficient of rainwater content has a similar magnitude to the magnitude of liquid CWC [20]. Thus, even in the case of clouds containing rain, the LWP is expected to be reasonably estimated using TB36, assuming the presence of cloud liquid particles only. This assumption is confirmed by synthetic experiments in Section III.

C. Microwave Transfer Characteristics Over Land and Ocean

To consider interactions between microwave and atmosphere including clouds, particular attention is needed regarding the difference in surface type (land/ocean), which largely affects the behavior of microwave radiative transfer through the atmosphere. Over the ocean, the surface radiation is much weaker compared to land at 36.5 GHz. The weak incoming radiation from the surface results in lower absorption. Thus, the emission by hydrometeors predominates over absorption and scattering of radiation from the ocean surface. Therefore, 36.5-GHz microwaves, which are less scattered, tend to increase through a cloud layer over the ocean. At 89.0 GHz, the absorption and scattering by hydrometeors of microwaves predominate over emission because of relatively strong microwaves from the ocean surface. On the other hand, microwaves over land tend to decrease through a cloud layer regardless of frequency because of strong radiation from the land surface (see Fig. 1).

Over land, due to the relatively small signal of clouds at 36.5 GHz, LWP estimates with TB36 are susceptible to land state variability [21]. Accordingly, to guarantee sufficient accuracy of LWP estimation using 36.5-GHz microwaves, a more detailed representation of the land state is required than that using 89.0-GHz microwaves. Seto et al. [21] showed that the error in the representation of land emissivity should be below 0.015.

D. Polarization Characteristics of Brightness Temperature at 89.0 and 36.5 GHz at the Top of the Atmosphere

To explore the polarization characteristics of interactions between Earth's surface and hydrometeors and microwaves at 89.0 and 36.5 GHz, we conducted simulations with an RTM based on the four-stream fast model [22], which uses

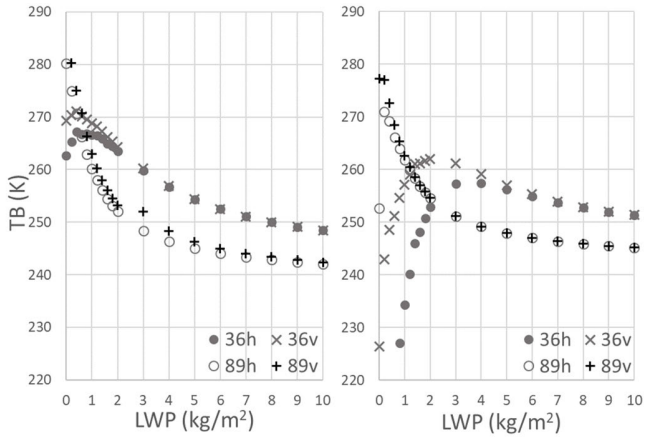

Fig. 2. Differences in brightness temperature (TB, K) between 36.5 and 89.0 GHz and horizontal (h) and vertical (v) polarizations at the top of the atmosphere calculated using the RTM with different LWPs (kg/m^2) over (left) land and (right) ocean.

the four-stream approximation method for radiative transfer calculation. We set the zenith angle for radiative transfer calculations to 55°, in accordance with the angle of the Advanced Microwave Scanning Radiometer for the Earth Observing System (AMSR-E) onboard the Aqua satellite. Inputs to the RTM include atmospheric profiles and lower boundary conditions, such as land surface radiation and land emissivity (reflectivity). We selected these inputs from the simulation results of the Le36 system, which are described in Section V.

Fig. 2 shows the responses of TB89 and TB36 at the top of the atmosphere over land and ocean to changes in the LWP. TB89 monotonically decreases as the LWP increases, whereas TB36 reaches a maximum value. This result indicates that although the LWP corresponding to a particular TB89 value can be determined using a single polarization, the LWP corresponding to a particular TB36 value may require both polarizations.

These considerations support the possibility of an algorithm for the estimation of LWP over land based on the frequency and polarization characteristics of TB36 as follows. First, soil moisture, which is the dominant factor influencing land emissivity, is estimated using low-frequency microwaves. Land radiations at both 36.5 and 23.8 GHz are calculated by the land RTM with the estimated soil moisture. Then, the LWP over land is estimated using the sum of both polarizations of observed TB36, with land radiation as background information. At the LWP estimation step in Le36, the use of TB23 to modify the water vapor condition is more effective for improving the accuracy of LWP estimation, similar to Le89 [16].

Based on the above concepts, a method for estimation of LWP over land can be developed using 36.5-GHz microwaves.

III. Systematic Development of LWP Estimation Using 36.5-GHz Microwaves Over Land

The LWP estimation procedure for Le36 over land is composed of the following four steps.

Step 1: Prediction of prior information about the atmosphere and land with atmospheric and land surface models that are used as inputs for atmosphere and land RTMs.

Step 2: Estimation of the optimal value of soil moisture using TB6 and TB10 observed via satellite, along with prior

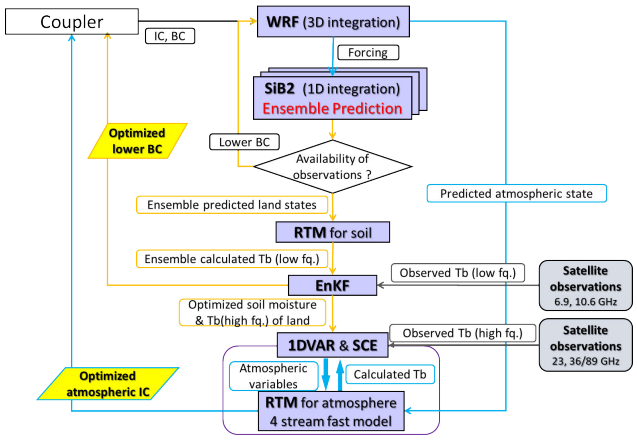

Fig. 3. System description (modified from [23, Fig. 1]).

information regarding land state (predicted in Step 1 through an optimal estimation algorithm).

Step 3: Calculation of TB23 and TB36 from the optimized land state using an RTM for land.

Step 4: Estimation of LWP, air temperature, and water vapor within clouds using the difference in TB23 and TB36 observed via satellite and calculated for land in Step 3, along with prior information regarding the atmosphere (predicted in Step 1).

The Le36 system consists of six components (see Fig. 3): a numerical weather prediction model, Weather Research and Forecasting (WRF), version 3.3 [24]; a land surface model, Simple Biosphere Model, version 2 [25], [26]; an RTM for land; an RTM for atmosphere and clouds; and optimal estimation algorithms for land (soil moisture) and atmosphere (LWP, water vapor, and temperature). The main program (coupler) combines these six models and algorithms online, and it controls the entire system. When satellite data are available, the coupler reads and transfers the data to the optimization algorithms. The coupler also sequentially passes variables among the six components (e.g., lower boundary conditions for the atmospheric model), forcing data for the land surface model, prior information for RTMs, and optimal land and atmospheric states for the models. Land and atmospheric interactions are reflected in these data exchanges. For radiative transfer calculations of land, a physically based RTM is used, which Kuria et al. [27] and Lu et al. [28] confirmed can be applied to the surface scattering of microwaves over a wide range of frequencies (from 6.925 to 89.0 GHz). For the atmospheric RTM, the four-stream fast model [22], which uses the Henyey–Greenstein scattering phase function with the four-stream approximation and plane-parallel atmosphere assumption, is utilized. The optimal estimation algorithm for land is based on the ensemble Kalman filter [29]; the algorithm for cloud and atmosphere is based on the 1-D variation method. To find the minimum value of the cost function of 1-D variation, we use shuffled complex evolution (SCE) [30], which is suitable for nonlinear cost function minimization. The temporal evolution of the atmosphere is calculated in three dimensions by WRF; the other calculations (land prediction and optimizations of land and atmosphere) are performed in one dimension for each grid. Satellite microwave data are set to model grids using the near-neighbor method. Ensemble predictions are conducted for land calculation.

LWP is estimated through the following procedures.

Step 4-1: The SCE method is used to select several values of LWP from among the values below an upper limit that is established in advance.

Step 4-2: The vertical distribution of liquid CWC is determined. Here, the vertical shape of CWC is considered parabolic. Water vapor and temperature within clouds are modified in physical association with the CWC value at that height; the atmospheric profiles are updated by saturating the water vapor in the cloud region according to the selected LWP values from SCE and considering the temperature change equivalent to the latent heat.

Step 4-3: From the determined CWC values and atmospheric profile, TB23 and TB36 at the top of the atmosphere are calculated by the RTM, and a cost function is calculated in the following form:

$$J(x) = \left(H(x) - y^o\right)^T R^{-1} \left(H(x) - y^o\right) = \left(T^{36}_{b,\text{est}} - T^{36}_{b,\text{obs}}\right)^2 + \left(T^{23}_{b,\text{est}} - T^{23}_{b,\text{obs}}\right)^2 \quad (1)$$

where x is the vertical distribution of CWC, water vapor, and temperature; H is a nonlinear observation operator; y^o is the observed brightness temperature; and R is the observation error covariance matrix, which is set to a unit matrix in this study. $T^f_{b,\text{est}}$ and $T^f_{b,\text{obs}}$ denote the calculated and observed brightness temperatures at a frequency of f, respectively. The difference between brightness temperatures is calculated for both horizontal and vertical polarizations.

Step 4-4: Until the value of the cost function decreases below the threshold, Steps 1–3 are repeated, and the optimal LWPs are estimated.

Simultaneous estimation of the LWP and the atmosphere within clouds can avoid the depiction of a physically improbable atmospheric state in the cloud system, such as extremely dry or cold conditions within the cloud. Furthermore, this method enables the TB23 signal to be effectively utilized although it is sensitive to water vapor. Detailed explanations of LWP estimation over land, including the atmospheric modification process within clouds, are available from the literature [16], [23].

IV. Synthetic Simulations of LWP Estimation Over Land Using Satellite-Based 36.5-GHz Observations

In this section, we describe a synthetic simulation that was conducted to test the viability of the proposed method of LWP estimation using TB36 without higher frequency measurements by investigating the scope of its application and limitations.

A. Simulation Descriptions

A synthetic simulation was conducted to explore the following three questions. How much LWP can be estimated by the method using TB36 with appropriate land representations? How sensitive is the estimation accuracy of Le36 to the uncertainty in cloud top (CT) height and vertical profile of CWC? Can the method be applied to the case of clouds containing rain?

In the synthetic simulation, there are two steps. First, we create synthetic TB36 and TB23 (hereafter, TB36_syn and TB23_syn, respectively) using the RTM from "true" conditions of the atmospheric profile (water vapor, air temperature, and air pressure), cloud water profile (LWP, shape of vertical distribution, and hydrometeor types), cloud layer, and land radiation. Second, using TB36_syn and TB23_syn, LWP is estimated by the procedures described above (Steps 4-1–4-4).

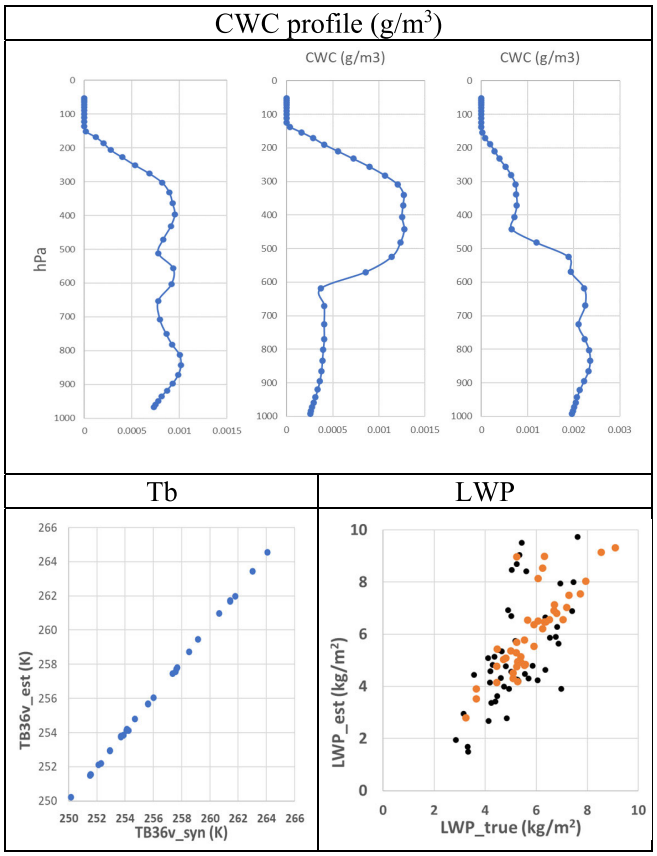

Fig. 4. (Top) Examples of CWC profiles for WRF-VP cases. (Bottom) Comparisons of (left) TB36_syn and TB36_est and (right) LWP_true and LWP_est. The red marks in the bottom right figure are the results of estimations using the same shape of vertical distributions in both Steps 1 and 2.

In the first step, to fulfill the three goals of this simulation, we test the sensitivity of LWP estimates to settings of LWP, CT height, vertical profile of CWC (VP), and hydrometeor constitution (HC) in "true" conditions. With respect to land radiation (mainly determined by soil moisture and soil temperature), the effects of uncertainty of land radiation in the Le36 are considered smaller than that of settings of CT and HC on uncertainties of LWP estimation. This is suggested by the estimated results of land surface radiation presented in Section V-C.

Settings of "true" LWP (LWP_true), CT (CT_true), VP (VP_true), and HC in synthetic simulations are shown in Table I. There are two cases for VP. In the first case (WRF-VP case), VPs from WRF simulations are used as VP_true, where the other settings (CT, HC, and LWP) are also as in WRF simulations. In this case, we conducted 50 simulations using different vertical distributions of CWC extracted from WRF simulations. Examples of CWC profiles for the WRF-VP case are shown in the top figures of Fig. 4. In the second case (Para-VP case), parabolic distribution is used as VP_true because Le36 assumes the vertical shape of CWC as parabolic. Moreover, in the second VP case, there

TABLE I
SYNTHETIC SIMULATION SETTINGS

		settings of "true" conditions (1st step)				settings of conditions for estimation (2nd step)				
Name		VP_true	HC_true	LWP_true	CT_true	VP	HC	LWP_est	CT	Atmospheric profile
WRF-VP		from WRF (50 different profiles)	from WRF	from WRF	from WRF	shape of VP_true	only cloud	estimated	same as CT_true	from WRF
Para-VP	Case C-1t	Parabolic distribution	only cloud	80 settings for each (from 0 to 8 in units of 0.1 kg/m^2)	pattern#1: 10 settings (from 5200 to 9700 in units of 500 m)	Parabolic distribution	only cloud	estimated	same as CT_true	10 profiles for each
	Case C-1c								constant (9000 m)	
	Case C-2c				pattern#2: 10 settings (from 9000 to 9900 in units of 100 m)				constant (9500 m)	
	Case CR-1t		cloud and rain (20% LWP for rain)		pattern#1: 10 settings (from 5200 to 9700 in units of 500 m (7200 to 9700 for LWP below 2.5 kg/m^2))				same as CT_true	
	Case CR-1c								constant (9000 m)	
	Case CR-2c				pattern#2: 10 settings (from 9000 to 9900 in units of 100 m)				constant (9500 m)	

are two cases for HC: Case C (LWP is composed of cloud liquid water alone) and Case CR (20% of LWP is composed of cloud liquid water, and the remainder is composed of rain). In Case CR, the vertical distribution of rain water content is determined such that it is maximized at the cloud bottom and decreases linearly to zero at the land surface and CT in Step 4-2. For each HC case, LWP_true is set to 80 values (from 0.1 to 8 in units of 0.1 kg/m^2). In Case C, CT_true is set to ten values (there are two patterns of setting: pattern#1 ranges from 5000 to 9500 in units of 500 m and pattern#2 ranges from 9000 to 9900 in units of 100 m). In Case CR, CT_true is set as for Case C but higher than 7200 m for LWP below 2.5 kg/m^2 because cloud systems with large LWP and sufficient rainwater to bring rainfall are expected to have high CT heights. Low settings of CT_true are unrealistic, leading to extremely high TB36_syn. Cloud bottom height does not have a particularly large sensitivity [31]; thus, it is set to a constant value (1500 m). The atmospheric profile used for the "true" conditions is common to all settings of LWP, CT, and HC.

In the second step (i.e., the estimation step), the estimated LWP (LWP_est) is assumed to be composed of cloud liquid water alone. CWC is assumed to be vertically distributed in a parabolic shape in all simulations except for one case in the WRF-VP cases, where the vertical distributions match the shape of VP_true (from the WRF simulation).

In WRF-VP cases, CT atmospheric profiles are set to the same as those from WRF simulations. In Para-VP cases, CT is set to the same value as CT_true or to constant values, enabling the investigation of sensitivity to errors in CT settings. For constant values, 9000 m is used for pattern#1 and 9500 m is used for pattern#2; accordingly, errors in CT vary from 0 to 4000 m. Regarding atmospheric profiles, ten profiles are randomly selected from profiles over land during prior or initial stages of a rainfall event in July in Japan. Different atmospheric profiles from profiles in the step to create synthetic observations are used to represent random errors in the step of LWP estimation. Table I shows the simulation conditions and their names in the second step.

B. Results and Discussion

Bottom figures in Fig. 4 show comparisons of synthetic observations (TB36_syn) and simulated TB36 (TB36_est) with estimated LWP and atmospheric profiles (shown in the bottom left figure) and true LWP_true and LWP_est (shown in the bottom right figure) for WRF-VP case. TB36_est adequately corresponds to TB36_syn, with errors of 0.15 K. This indicates that the performance of the numerical procedure for the minimum search of the cost function is sufficiently high for our focusing optimization problem.

In the WRF-VP case, the estimation of LWP resulted in an average error of approximately 1.4 kg/m^2, with an error of about 25% (bottom right figure). This outcome indicates the impact of differences in the vertical distribution of CWC, including hydrometer type (cloud or rain) and shape of the distribution, on the accuracy of LWP estimates. In Step 2 of this simulation, the CT values were set to the same values as CT_true, which were determined from WRF's CWC profile. The influence of errors in the CT setting is addressed in the Para-VP case. While some variability is observed, reasonable values for LWP are estimated within the range shown in the figures. However, compared to the case where the same shape of vertical distributions is used in both Steps 1 and 2 (red mark in the figure), it becomes apparent that errors are larger, and the profile shape is one of the contributing factors to these errors. In comparison to the parabolic distribution, it notably differs in the presence of abundant precipitation near the surface, especially during heavy rain. On the other hand, signals from hydrometeors near the surface are relatively small, which is believed to contribute to the underestimation of LWP.

Fig. 5 shows the results of synthetic simulations of Case C (Cases C-1t, C-1c, and C-2c) of the Para-VP case. The top figures are comparisons between TB36_syn and TB36_est; the bottom figures show LWP_true and LWP_est. With respect to the results of brightness temperature, TB36_est adequately corresponds to TB36_syn in all three cases, as in the WRF-VP case, with errors below ∼0.1%. With the perfect CT setting (Case C-1t), LWP is estimated with high accuracy, involving mean errors of ∼12% for a wide range of LWP values (0–8 kg/m^2). In particular, using an atmospheric profile input identical to the first step (red plots), the accuracy is rather high (mean error of 1.7%).

For Case C-1c, results with CT_true of 8700 and 9200 are indicated by gray marks in Fig. 5, CT_true from 6700 to 8200 indicated by blue marks, and CT_true

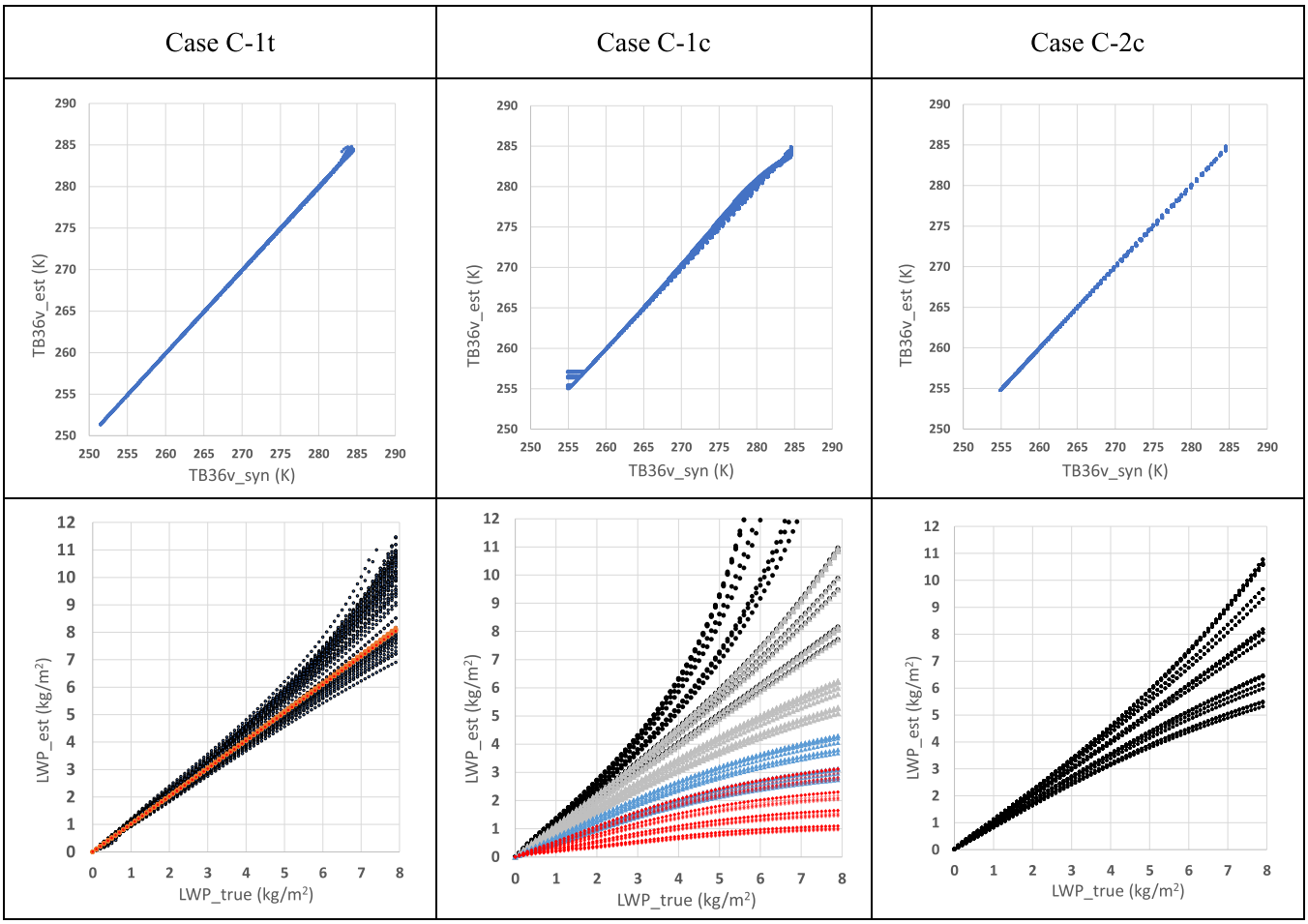

Fig. 5. Comparisons of (top) TB36_syn and TB36_est and (bottom) LWP_true and LWP_est for Cases C-1t, C-1c, and C-2c. There are 8000 plots for each case. Red plots in Case C-1t are results using the same atmospheric profile input as the first step. In Case C-1c, gray plots are results with CT_true between 8000 and 9000, blue plots are results with CT_true between 7000 and 8000, and red plots are results with CT_true below 7000.

below 6700 indicated by red marks. These results reveal that larger errors in CT settings lead to larger errors in LWP estimation; the sensitivity of LWP estimation to the CT setting is very high, consistent with findings by Seto et al. [16]. Our method uses a constant high value of CT at the estimation step; thus, the accuracy becomes low when the target cloud's top height is low. For the case of large LWP_true, the errors are large. Generally, the CT of clouds with large LWP tends to be high. Therefore, our method with a constant CT setting is applicable to high-CT cases or thick-cloud cases, but some constraints for the CT setting are desirable. Compared with the WRF-VP case, it becomes evident that differences in CT height have a more significant influence on the uncertainty of LWP estimates compared to variations in the shape of vertical distribution and hydrometeor type.

Case C-2c is conducted for a case where some information about CT is obtained from other sources including infrared observations of geostationary satellites. The mean error for all LWP_true is 10.1%. The error of LWP estimation becomes large when LWP_true is large. When LWP_true is >6 kg/m^2, the mean error is 14.8%. The results of Case C-2c indicate that to estimate LWP using TB36 with sufficient accuracy for no-rain clouds, it is desirable that the CT can be set with an error of <500 m using other satellite-based observations; in that case, Le36 can be applied to a wide range of LWP values.

In Case CR of Para-VP case (see Fig. 6), similar to Case C, TB36_est and TB36_syn exhibit good agreement in all three cases, except when TB36_syn is higher than 285 K. TB36_syn becomes >285 when CT_true is set to low values such as 5200 and 5700 m or when LWP_true is between 0.3 and 1.5 kg/m^2 (simulated TB36 becomes the maximum value with these LWPs over land; not shown). The results of LWP estimation are also not good for this range of LWP.

The reason for this disagreement is thought to be as follows. In general, it is known that there is difficulty in estimating small LWP over land because strong land radiation eliminates the signals from clouds with small LWP due to the incompleteness of the representation of land radiation. However, in synthetic simulations, we consider land surface radiation to be perfect, so the issue of land surface radiation is eliminated, and what remains is the problem of radiative transfer within the clouds. When comparing the results of Case C-1t and Case CR-1t, it can be found that Case CR-1t does not estimate LWP values within the range of 0.3 to 1.5 kg/m^2, whereas Case C is capable of estimating LWP within this range. From this, it can be understood that the reason why Case CR-1t fails to estimate LWP effectively within the range of 0.3–1.5 kg/m^2 is due to the assumption of estimating LWP, including rain, as containing only cloud water. In clouds that contain raindrops, there are cases where net radiation is slightly increased even over land when LWP

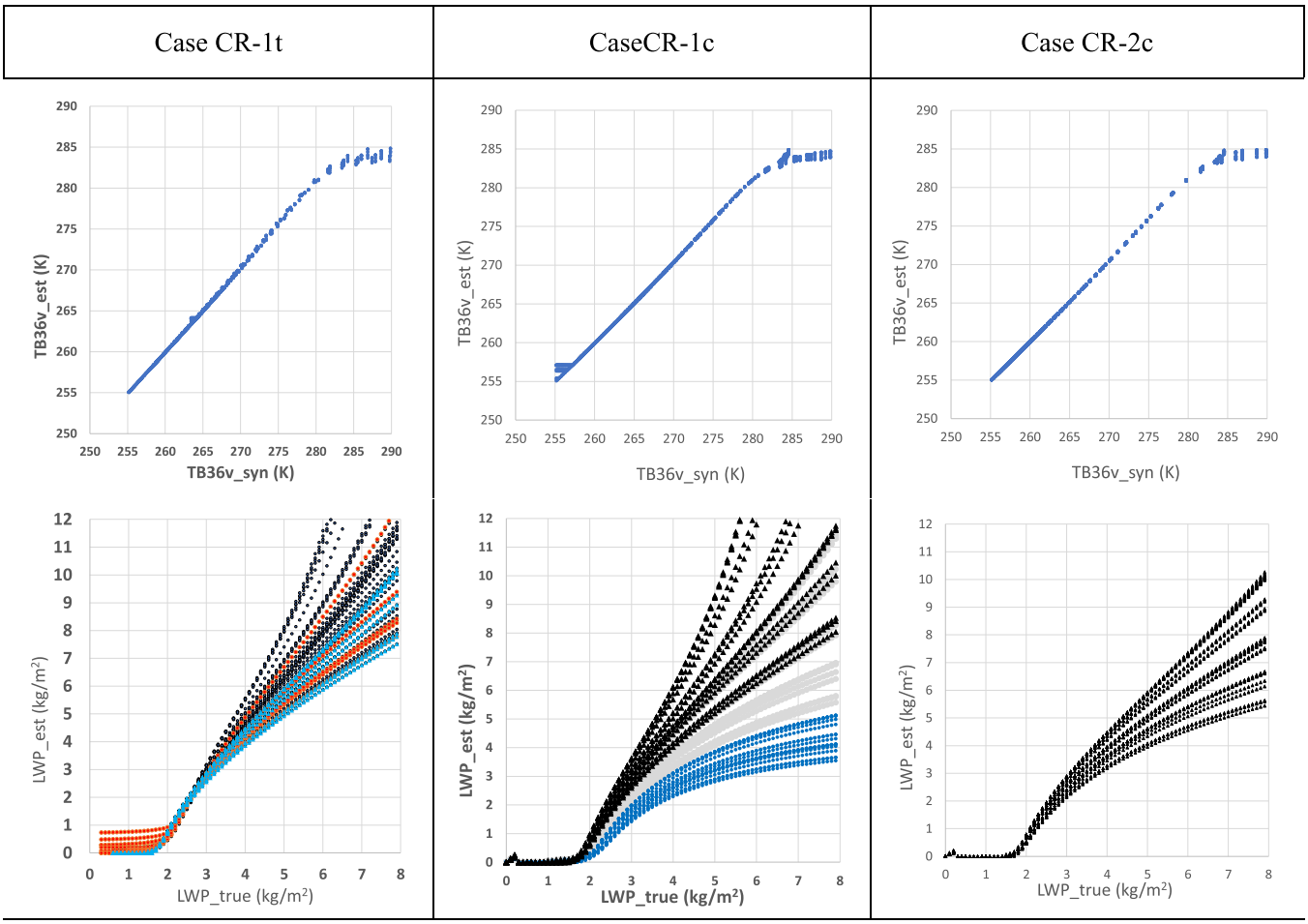

Fig. 6. Same as Fig. 5, but for Cases CR-1t, CR-1c, and CR-2c.

is relatively small, albeit to a lesser extent. On the other hand, no-rain clouds fundamentally attenuate land surface radiation, which is believed to be the cause of such discrepancies.

For cases with both cloud and rain, errors are high compared with cloud-only cases, even when using the perfect CT setting (Case CR-1t). The error averaged over all samples is 35%. In particular, errors are large when CT_true is low and LWP_true is larger than ∼4 kg/m^2. The main cause of this large error is the unrealistically low setting of CT_true for precipitating clouds, including large LWP and estimated high TB36_syn by the RTM. With a CT_true of 9700 m, the results are much better; the error is 19% (blue plots in Fig. 6).

For Case CR-1c, the results were similar to Case C-1c. When the difference between CT_true and CT_est is large and LWP_true is large, errors in LWP estimation also become large, and the sensitivity of LWP estimation to the CT setting is rather high. However, when errors in the CT setting are <1000 m, estimation errors are ∼25% (gray plots). This result indicates that our method (using high constant CT value) is applicable to clouds with large LWP including cloud and rain; in most such cases, CT is high.

The results of Case CR-2c indicate that this method can accurately estimate LWP including cloud and rain, with a mean error of ∼20%, if CT can be set to an appropriate value using CT information obtained by other satellites.

According to the comparison between the TB36_syns of Cases C and CR (see Fig. 7), the difference is small in the range of LWP > 3 kg/m^2 and not much larger in the range of LWP > 2 kg/m^2. For cases with relatively large LWP, which are realistic values for cloud and rain cases, the assumption that LWP comprises cloud water alone is acceptable.

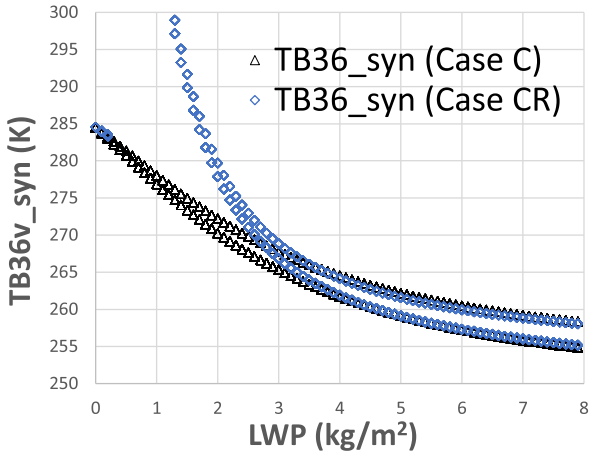

Fig. 7. Comparison between TB36_syns of Cases C and CR.

In summary, the LWP estimation method over land with TB36 can be applied to clouds with a wide range of LWP (∼8 kg/m^2) for cloud-only cases if the CT setting is appropriately constrained by independent CT information. While the impact is smaller compared to cloud-top height, the shape of CWC's vertical distribution is also one of the contributing

factors to errors. For cloud-plus-rain cases, LWP retrieval shows good performance in the range of about 1.5–8.0 kg/m^2, even if with CT information. In cases without CT information, this method can be applied by limiting the targets to high CT heights (approximately 8000 m and above). However, it is desirable to utilize CT height information from other sources. The use of satellite-based infrared observations is considered effective for obtaining CT height information. Therefore, the proposed method using 36.5 GHz is suitable for estimating clouds over land that produce relatively strong rain (LWPs exceeding 1.5 kg/m^2) or rain-free clouds, and for cases of clouds of smaller LWPs accompanying rain, it is necessary to consider the combination of other frequencies.

V. Application of Le36 to Real Cases

The developed method (Le36) was applied to real cases, and the performance was investigated by comparing the results of Le36 with the results of Le89. Independent satellite cloud radar products are also used for discussion.

A. Data

The microwave data used for estimation are the brightness temperatures measured with the AMSR-E located on the Aqua satellite. Although both Le89 and Le36 can use microwave data measured with AMSR2 (currently in operation), AMSR-E (completed operation) is utilized because the target periods used for validation align with the operation period of CloudSat. Le36 uses four frequencies (6.925 and 10.65 GHz for land estimation; 23.8 and 36.5 GHz for atmosphere and LWP) among six total frequencies (6.925, 10.65, 18.7, 23.8, 36.5, and 89.0 GHz) observed by AMSR-E. In this study, to elucidate the performance and characteristics of LWP estimation using 36.5 GHz, 89.0 GHz is not used with Le36, whereas Le89 uses 89.0 GHz, rather than 36.5 GHz.

The footprint for observation at 36.5 GHz is larger than the footprint at 89 GHz (approximately 10 and 5 km, respectively); therefore, land and ocean data are more frequently included within a single footprint. These mixed land/ocean signals lead to incorrect estimation. In Le36, observed TB36 is modified prior to calculation according to the ratio of land and ocean as follows. The brightness temperature observed with AMSR-E, Tb (AMSR), is described using the ratio of land within the footprint, a, and the brightness temperatures of land and ocean, Tb (land) and Tb (ocean), respectively, as

$$\mathrm{Tb(AMSR)} = a \times \mathrm{Tb(land)} + (1-a) \times \mathrm{Tb(ocean)} \quad (2)$$

If the cover of a model grid is land, the observed brightness temperature is modified as

$$\mathrm{Tb(land)} = \{\mathrm{Tb(AMSR)} - (1-a) \times \mathrm{Tb(ocean)}\}/a \quad (3)$$

where the value of Tb(ocean) is determined by searching the nearest grid of $a = 0$ and using its brightness temperature. However, because this modification may wrongly discard the signal in grids with clouds, the modification is not applied to such grids. We determined whether a cloud signal is present in each grid using observed TB89.

Le36 uses both horizontal and vertical polarizations based on the radiative transfer characteristics of 36.5 GHz, as discussed in Section III.

We used products from the CloudSat satellite as references to validate and discuss the features of LWP estimates from Le89 and Le36. CloudSat carried the W-band cloud profiling radar (CPR), which measured backscattering by clouds as a function of distance from the radar. CPR provided unprecedented data regarding cloud microphysics with a vertical resolution of 485 m and a footprint of 1.4 km (cross-track) × 2.5 km (along-track) [32]. CloudSat flies in orbital formation as a component of the constellation of satellites known as the A-train, which sequentially orbit in the same orbital plane at close spacing. The A-train also includes the Aqua and Global Change Observation Mission—Water (GCOM-W) satellites. Aqua is equipped with AMSR-E, which is used for estimation in this study; a successor of AMSR-E, known as AMSR2, is onboard GCOM-W. Thus, CloudSat products were appropriate for our target.

Cloud microphysical data are included in the 2B-CWC-RO, 2B-CWC-RVOD, and 2C-ICE CloudSat products. In this study, 2B-CWC-RVOD version R04 products and 2C-ICE version R04 products were used to investigate the validity and features of LWP estimated using Le89 and Le36. As indicated in level 2B-CWC-RO P_R04 data issues, 2B-CWC-RO data include many unsuccessful retrievals of liquid water content, particularly in profiles with high radar reflectivity related to the presence of large raindrops. These gaps occur because the retrieval procedures do not converge when the observed reflectivity is greater than the range allowed by a priori data, resulting in water content with very high attenuation [33]. In the retrieval algorithm for 2B-CWC-RVOD products, the optical thickness estimated from visible channels of the Moderate Resolution Imaging Spectroradiometer onboard the Aqua satellite is used as a constraint for optimization calculations, along with reflectivity measured via CPR. Therefore, 2B-CWC-RVOD contains fewer missing data. Because this study targeted cloud systems containing a large quantity of hydrometeors, we used 2B-CWC-RVOD products, rather than 2B-CWC-RO products.

For the 2B-CWC-RVOD algorithm, separate retrievals were initially performed under the assumption that the entire cloud column was liquid only or ice only. Then, the two sets of results were combined into a composite profile according to a simple temperature relationship. The ice retrieval solution was applied to heights where the temperature was below −20 °C (only ice was present); the liquid solution was applied to heights where the temperature was above 0 °C (only liquid was present). A linear combination of the two was used for the intermediate temperature range (mixed cloud was present). Because we also assumed that entire clouds were liquid at the time of estimation, we used ice and liquid water contents and only-liquid part of the water contents from 2B-CWC-RVOD products for LWP comparison. Hereafter, the sum of liquid and ice water paths is called CS_RVOD, and LWP is called CS_RVOD_liq. CloudSat products are rare and valuable data for LWP evaluation over land and used in real-case simulations, but the results should be discussed in conjunction with synthetic simulations, considering the inconsistency between CloudSat products and these assumptions in product generation. More detailed descriptions of 2B-CWC-RVOD data are provided in the CloudSat Data Processing Document and the report by Austin et al. [34].

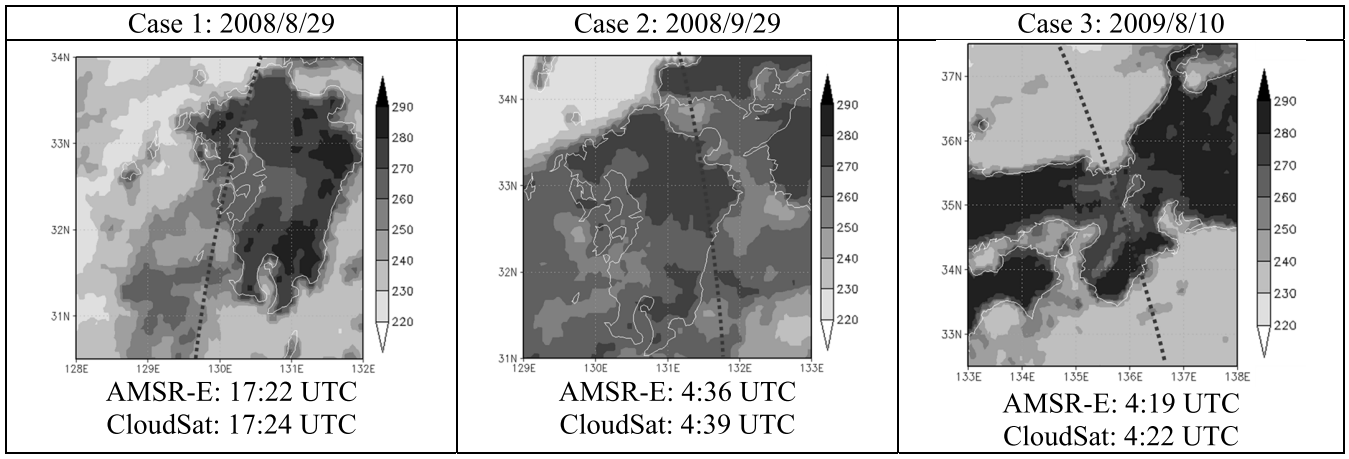

Fig. 8. Date, area, and observation time for target cases. Shaded area: TB36 (K) observed using horizontal polarization. Dashed line: path of CloudSat satellite.

TABLE II
EXPERIMENTAL SETTINGS (FOR LE36 AND LE89)

	Use of TB observations	Cloud height in estimation (Top : Bottom)	Sensitivity test
Es_CTL	No	No	No
Es_AM	Yes	10,000 : 1500 m	Changing TB until ± 2 K in 1-K increments
Es_CS	Yes	Determined from CloudSat	Changing cloud top until ± 1000 m in 200-m increments

We used 2C-ICE data for one case where most of the ice water content of 2B-CWC-RVOD was missing. The 2C-ICE product is created using radar reflectivity from CPR onboard CloudSat and lidar backscattering data from Cloud-Aerosol Lidar and Infrared Pathfinder Satellite Observation (CALIPSO) [35], [36]. Several ice-cloud retrieval products have been evaluated with in situ measurements [37], which showed that the 2C-ICE product had better agreement with in situ data than with 2B-CWC-RVOD. In the cases of this study, 2C-ICE largely overestimated ice water content relative to 2B-CWC-RVOD. Thus, we use this product for reference. Hereafter, the sum of LWP from 2B-CWC-RVOD and ice water path from the 2C-ICE product is called CS_ICE.

For data comparison, CloudSat and LWP data from Le36 and Le89 were converted at the same grid scale. The method used for this conversion was described in [16].

The National Centers for Environmental Prediction (NCEP) Final Operational Global Analysis data were used for initial and boundary conditions of larger domains to calculate prior information.

B. Experimental Settings

In this study, we applied Le36 and Le89 to actual cases and compared their performances. Based on that comparison, we discuss the characteristics of LWP estimation using microwave radiation at 36.5 GHz.

1) Target Cases: We selected three cases, as shown in Fig. 8. We selected study cases based on the following criteria: the availability of CloudSat products—2B-CWC-RVOD data were only available through April 2011 because of a battery anomaly and the satellite's corresponding exit from the A-train formation (see CloudSat Epochs Information, provided by CloudSat data processing center on their website); the availability of CloudSat products containing appropriately large (thick) clouds; the availability of CloudSat products over land at low latitudes to midlatitudes—most of the CloudSat orbit passes over oceanic and polar regions; and the availability of AMSR-E data—AMSR-E data were only collected through 2011.

Fig. 8 shows the horizontal distribution of TB36 observations by AMSR-E and the path of CloudSat at the time corresponding to each case. The observation time differences between AMSR-E and CloudSat are 2–3 min for all three cases.

2) Settings Used for Estimation: We compared the results obtained under three different settings, as shown in Table II. Hereafter, the first setting with no observations is called Es_CTL. This setting simply returns prediction results from the coupled atmosphere and land models.

Second, we estimate LWP using brightness temperatures observed by AMSR-E (hereafter called Es_AM). For this method, we used fixed heights of the CT (10 000 m) and cloud bottom (1500 m) to constrain the vertical distribution of CWC. In addition, using Es_AM as a reference experiment, we conducted sensitivity tests by changing the TB values at 36.5 and 23.8 GHz (i.e., frequencies used for cloud estimation in Le36), in steps of 1 K from −2 K to +2 K relative to the observed values.

The third method used CT and bottom heights determined from CloudSat products as additional constraints for LWP estimation, in addition to AMSR-E observations. Hereafter, this setting is called Es_CS. The Es_CS method was used to determine the extent to which cloud layer information would improve LWP estimation, according to the conclusions obtained from synthetic simulation in Section IV. The CT and cloud bottom heights in Es_CS were determined according to the CloudSat product (CS_RVOD) for each profile. When CWC was >0.2 g/m^3, that height was included in the cloud

TABLE III
MODEL SETTINGS FOR LE36 AND LE89

Horizontal resolution		5 km
Time step		Land: 10 min; atmosphere: 30 s
WRF parameterization	**Radiation**	RRTMG
	Boundary layer	Mellor–Yamada level: 2.5
	Cloud microphysics	WSM6

layer. We used CT and cloud bottom heights from CloudSat for model grids with CloudSat profiles $< 0.02°$ in direct distance from the model grid; the horizontal resolution of the model was 0.05°. If appropriate cloud layer data were not available for a profile, for example, because of missing data around cloud boundaries or a lack of CWC, default values were used for the profile, similar to Es_AM. For Es_CS, we also conducted sensitivity tests by changing CT height in a stepwise manner with 200-m steps from −1000 to +1000 m, relative to the CT height used in Es_CS. These sensitivity tests provide information regarding the uncertainty of this method.

All other settings were held constant among all cases and methods, as shown in Table III. The number of ensemble members for the land model integration was set to 50, which is sufficient to represent the error distribution for three-layer and 1-D soil moisture. Because of the lack of observational evidence, the observational error covariance matrix was empirically set to a diagonal matrix. Boundaries of LWP for estimation, used to select the LWP value in the SCE minimization process, were determined from the maximum value of vertically integrated total (liquid and ice) water content in the results of a WRF run covering several months including the target period; they were set to 0–15 kg/m^2.

C. Results of LWP Estimation by Le36

In this section, we discuss the performance of Le36 and the feasibility of liquid cloud and rain partitioning; we mainly focus on the results of Case 1 because similar results were obtained for Cases 2 and 3 (refer to the Appendix).

1) Brightness Temperature: Fig. 9 shows TB6 distributions observed by AMSR-E (top figure), calculated by Le36 before land estimation (middle left figure), and after estimation (middle right). Scatter plots of observed and calculated TB6s are also shown (bottom figures). The target area consists of multiple land and vegetation types (e.g., grassland, needleleaf-evergreen trees, and broadleaf shrubs with bare soil). The results demonstrate that the land surface radiation can be well reproduced regardless of the land surface type. Furthermore, as the estimation of land parameters and LWP is performed independently at each location, the method has shown reasonable reliability in terms of the validity of its performance regarding various land parameters and surface types. However, during the target period in this area, there was no snow cover and no frozen ground, so validation regarding this surface coverage has not been conducted.

Fig. 10 shows TB36 calculated by the RTM before and after LWP estimation by Le36. TB36 before LWP estimation is calculated using the atmosphere and CWC profile predicted by the WRF model. TB36 after LWP estimation, calculated using estimated atmosphere and CWC profiles, demonstrated

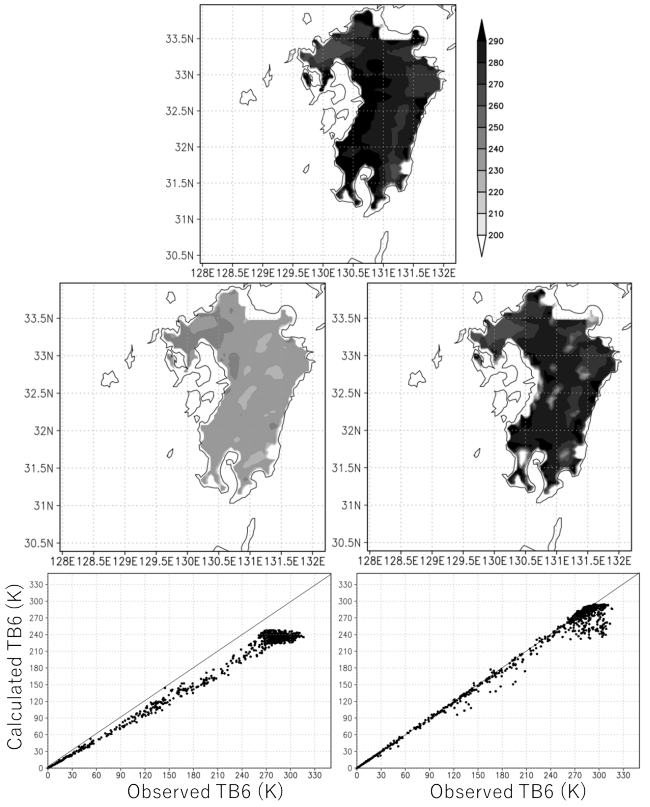

Fig. 9. TB6 (K) distributions observed by (top) AMSR-E, calculated by Le36 before land estimation (middle left figure) and after estimation (middle right), and scatter plots of observed and calculated TB6s (bottom left: before estimation; bottom right: after estimation).

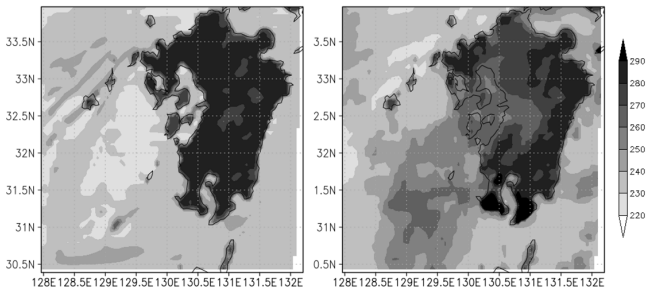

Fig. 10. TB36 (K) calculated using the RTM (left) before and (right) after cloud estimation.

a very accurate representation of the horizontal distribution of observed TB36 (as shown in Fig. 8) both over land and ocean.

To investigate the frequency dependence of radiative interactions of microwaves and clouds, TB89 values observed and calculated by the RTM after LWP estimation by Le89 are shown in Fig. 11. TB89 values calculated after LWP estimation were slightly higher than observed TB89 values. This disagreement indicates that the actual attenuation effect is greater

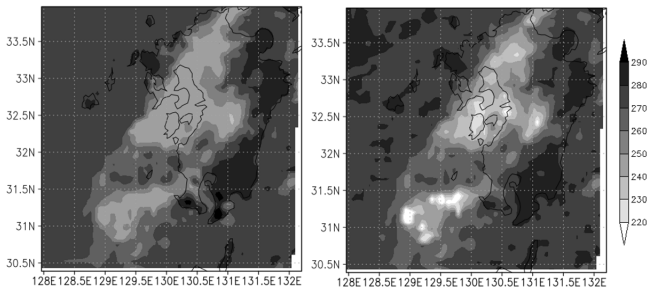

Fig. 11. TB89 (K) calculated using the RTM (left) after cloud estimation and (right) observed.

than the effect represented in Le89. We attribute the cause of this discrepancy to the following factors. As described in Section II, most attenuation by liquid cloud water particles is related to absorption. Also, as shown in Fig. 2, when the LWP is large, TB89 reaches saturation and shows little variation. In contrast, observed TB89 was affected by the scattering of ice cloud particles. Le89 estimated LWP assuming only liquid cloud water and did not reflect attenuation by ice cloud particles in the RTM calculation. Accordingly, Le89 could not represent a decrease in TB89 related to ice scattering within a realistic range of LWP; the predicted TB89 after LWP estimation was higher than the observed TB89. This result indicates that less liquid cloud particle-related attenuation occurred for TB89 compared with attenuation caused by ice cloud particles comprising the same amount of water. According to a comparison of results from Le36 and Le89, it is suggested that because TB36 included minimal signals from ice particles, Le36 can more accurately reproduce the observed brightness temperatures compared to Le89.

2) LWP: The results of LWP estimation by Es_AM and Es_CTL are shown for Le36 and Le89 in the top and bottom figures of Fig. 12, respectively, along with LWPs obtained from CloudSat products (CS_RVOD and CS_RVOD_liq). In these graphs, black solid lines represent LWP values from Es_AM, red solid lines represent LWP values from Es_CTL, and thick and thin blue (brown) lines represent LWP values from sensitivity tests subtracting (adding) 2 K or 1 K from (to) the TB36 results of Es_AM. Short-dashed lines represent LWP values from CloudSat, black lines indicate the CS_RVOD, and red lines indicate the CS_RVOD_liq. The horizontal axis is the number of profiles from south to north along the CloudSat path. Thick straight lines at the bottom of each figure indicate the land/sea flag (brown indicates land; blue indicates sea). For Case 3, ice water content is missing from 2B-CWC-RVOD at most of the target profiles; thus, CS_ICE is used (see the Appendix).

For Le36, the value of LWP from Es_AM shows a similar value to CS_RVOD_liq. The mean LWPs for all data points of Es_AM, CS_RVOD, and CS_RVOD_liq are 0.97, 2.7, and 0.97 kg/m^2, respectively. The root mean square error (RMSE) calculated between Es_AM of Le36 and CS_RVOD_liq (CS_RVOD) is 0.82 (1.84). While they do not necessarily match on all individual profiles, Es_AM and CS_RVOD_liq show good agreement on average for profiles. Based on a comparison of the horizontal shape of LWP (see Fig. 12), estimates from Es_AM of Le36 represent a similar shape to CS_RVOD (sum of liquid and ice water path).

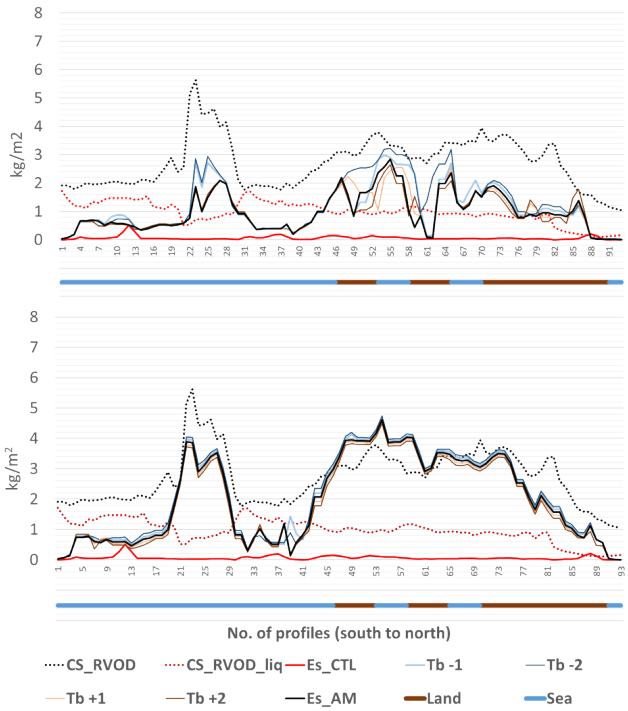

Fig. 12. Comparison of total LWPs from Es_CTL (red line), Es_AM (black lines), and cloud water paths from CloudSat products (black and gray short-dashed lines) along CloudSat paths. Thick and thin blue (brown) lines were obtained from sensitivity tests subtracting (adding) 2 K or 1 K from (to) TB36 from Es_AM. The thick straight line at the bottom indicates the land/sea flag (brown indicates land and blue indicates sea). (Top) Le36. (Bottom) Le89.

Top figures of Fig. 13 show scatter plots of LWPs from Es_AM of Le36 and Le89. The scatter plot also reflects similar results. The LWP values between Le36 and CS_RVOD_liq show a close average, but individual data points exhibit both overestimation and underestimation. On the other hand, when comparing Le36's LWP with CS_RVOD, there is an overall underestimation, but the values are still highly correlated. In the algorithm used to generate CS_RVOD_liq (liquid part of water content of CloudSat product), it assumes that all values below freezing are ice, which means that there is no contribution of cloud particles above the melting layer, and signals from these particles are excluded for CS_RVOD_liq. This is believed to result in a flatter horizontal distribution of LWP of CS_RVOD_liq.

LWP determined from Es_AM of Le36 is smaller than CS_RVOD_liq for grids with a relatively small value of CS_RVOD. A small value of CS_RVOD indicates a small cloud signal in CloudSat observation. The potential cause of this discrepancy can be described as follows. As the results of synthetic simulation indicate, the incorrect assumption of the distribution of cloud water and rainwater during LWP estimation makes it difficult to properly represent their dissipation processes when LWP is below about 1.5 kg/m^2, which means small cloud signals in TB36. This results in the underestimation of LWP. In real-case simulations, cloud is assumed to include only cloud water although actual clouds are supposed to include both rain and cloud. Thus, the observed TB36 is a little higher value than what can be expressed by the assumption of clouds alone, leading to a failure in estimating small LWP.

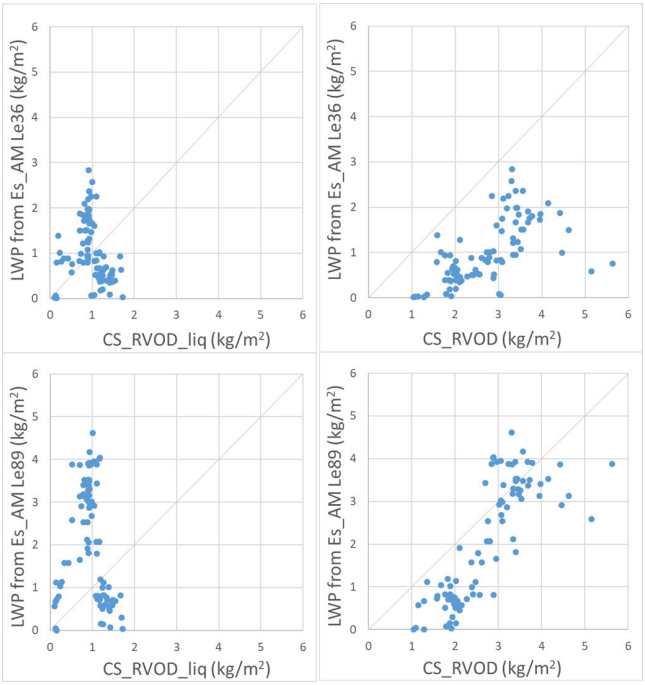

Fig. 13. Scatter plots of LWPs from CloudSat products [(left) CS_RVOD_liq and (right) CS_RVOD] and Es_AM of (top) Le36 and (bottom) Le89.

However, in the vicinity of profiles over land around No. 76–90 in Fig. 12, an LWP of approximately 1.0 kg/m^2 is estimated. Signals from clouds with these LWPs are much smaller than land radiation so that it is generally considered very challenging to observe small LWP values in land-based clouds. From this result, it can be suggested that depending on the condition (distribution of cloud and precipitation particles), the small LWPs can be successfully estimated by our method, which indicates that simultaneous estimation of the atmosphere and land states shows its effectiveness for small LWP cases.

Notably, Le36 successfully achieves continuous estimation of LWP over land and ocean without TB89. Thus far, microwaves at approximately 36.5 GHz have generally been used to estimate LWP over oceans or rainfall over land in conjunction with microwaves at higher frequencies, such as ~89.0 GHz. Estimation over land using 36.5 GHz alone is difficult because the cloud signal in microwave measurements at this frequency is much smaller than the signal from land radiation. Nevertheless, Le36 enables the estimation of LWP over land using only 36.5 GHz by appropriately and dynamically representing soil moisture, land emissivity, and land radiation. The use of Le36 reduces the amount of information needed for LWP estimation and supports the use of high-frequency microwaves for liquid and ice partitioning estimation.

The comparison of LWPs from Es_AM using Le36 and Le89 revealed that Le36 returned smaller values. The mean LWPs for all data points of Es_AM of Le89 are 1.98, and RMSE between Es_AM of Le89 and CS_RVOD_liq (CS_RVOD) is 1.82 (1.08). Similar to the results for brightness temperature, this finding indicates that Le89 estimated larger LWP values because TB89 includes a larger cloud signal driven by ice scattering. The LWP from Le89 is more similar to CS_RVOD compared with the LWP from Le36. Observed TB89 is strongly affected by ice scattering, but Le89 considers only liquid cloud particles. Thus, Le89 compensates for the attenuation effect by increasing LWP; the estimated LWP from Le89 is larger than the LWP from Le36 and similar to CS_RVOD. In addition, when the absolute value of LWP for a grid is high, the difference between LWP values from Le36 and Le89 is large. This relationship indicates that a cloud system with a large amount of water tends to demonstrate robust development and include a large number of ice particles. The difference between TB36 and TB89 will be large for such cloud systems. Le89 performs better in estimating LWP in grids with small signals, where CS_RVOD is smaller than 2.0 kg/m^2, around grids numbered 30 and 40. Thus, it can be inferred that combining TB89 with Le36 would be beneficial for estimating LWP in this range.

From the scatter plot of Le89 (bottom figure of Fig. 13), it can be observed that the estimated LWP values closely match CS_RVOD. However, there is a significant difference compared to CS_RVOD_liq, indicating a lower accuracy in estimating LWP.

Next, we focus on the results from sensitivity tests of LWP estimation conducted by changing TB36 (top figure of Fig. 12) and TB89 (bottom figure), as indicated by thick and thin blue and brown lines. Each line shows the results from an experiment adjusting the temperature (from −2 K to +2 K) to the observed brightness temperature. The results show that the sensitivity of LWP estimation to brightness temperature is higher for Le36 than for Le89; in particular, LWP substantially changes (several kilograms per square meter) over land and coastal oceans. These results indicate that the effect of clouds relative to the background radiation is smaller on TB36 than on TB89; In addition, the effect is smaller over land and coastal oceans than over open ocean areas. Observed TB36, as shown in Fig. 8, suggests weak cloud signals over land. These results indicate that error reductions in observations and representations of land radiation, which is used as background information, are essential for Le36 because of the high sensitivity of LWP estimation to TB36. The high sensitivity over coastal ocean areas may be related to the effect of mixing land and ocean areas within a footprint. In Section V-C3, we discuss the influences of mixed land and ocean signals within a footprint on LWP estimation.

The effect of including cloud height information as additional constraints on LWP estimation is examined using the results of Es_CS, which is shown by black solid lines in Fig. 14 and scatter plots in Fig. 15. For Le36, overall, LWP estimates from Es_CS are lower than from Es_AM; accordingly, the estimates well match CS_RVOD_liq. In Es_CS, LWP values around 1.0 kg/m^2 are well estimated at many locations. According to the results of synthetic simulation, when clouds and rain are mixed, small LWP values are not accurately estimated. Therefore, it is expected that in profiles with small LWP values in this case, there were fewer raindrops present. Around the grid numbered 46 (hereafter Grid46), LWPs are overestimated by 2~3 kg/m^2. The causes of overestimation here are examined in Section V-C3. Furthermore, overestimations in Le89 are also improved in Es_CS. In particular, in many grids over land, the LWP estimated in Es_CS is smaller than the LWP estimated in Es_AM. Changes in CT height influence emissions from clouds by changing the

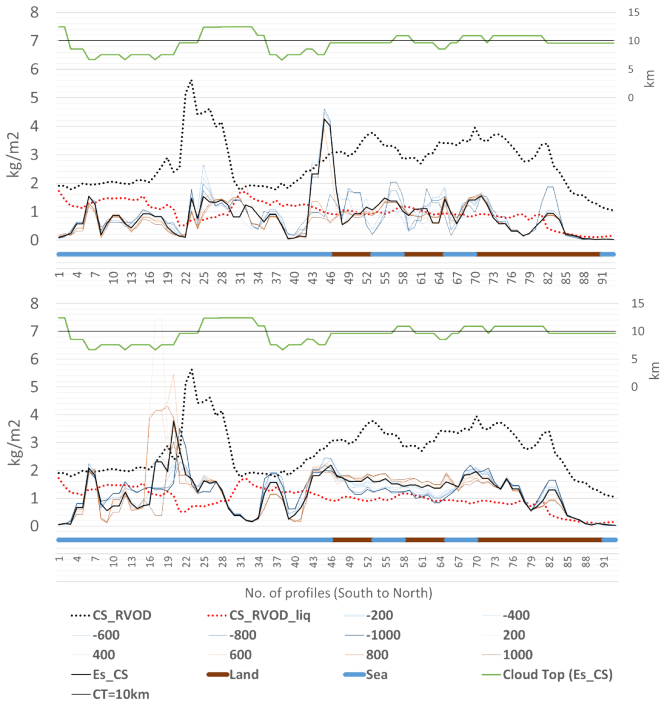

Fig. 14. Comparison of total LWPs from Es_CS (black lines) and cloud water paths from CloudSat products (black and gray short-dashed lines) along CloudSat paths. Thick and thin blue (brown) lines were obtained in sensitivity tests by subtracting (adding) 200, 400, 600, 800, or 1000 m from (to) CT heights from Es_CS. The thick straight line at the bottom indicates land/sea flag (brown: land; blue: sea). The green solid line in the upper part of the right axis represents CT heights determined from CloudSat using Es_CS. (Top) Le36. (Bottom) Le89.

physical temperatures of cloud particles. Clouds tend to reduce TB36 over land and increase it over the ocean, as described above. Thus, if the CT height descends by using CT information from CloudSat over land, absorption by clouds is increased; less LWP is required to obtain the same TB36 value over land. This feature is confirmed via synthetic simulation in Section IV. As indicated by green lines in Fig. 14, the CT height is lower in Es_CS than in Es_AM at many points. This is one likely reason why LWP is smaller from Es_CS than from Es_AM at these grids over land although there may be a more complex nonlinear relationship between CT height and TB36. On the other hand, over the ocean around grids numbered 4–22 and 30–40, it is the opposite situation, that is, lower CT results in higher LWP estimates because there is a net increase of radiation over the ocean. The mean LWPs for all data points of Es_CS are 0.84 and 1.17 kg/m^2 for Le36 and Le89, respectively.

The LWPs produced in each sensitivity experiment with varying CT heights are shown in Fig. 14. Thick and thin blue (brown) lines are from sensitivity tests subtracting (adding) 200, 400, 600, 800, or 1000 m from (to) the CT heights of Es_CS. For Le89, the sensitivity of estimated LWP to cloud height is higher than its sensitivity to TB89, indicating that the setting of CT height is more important to accurate estimation than the error in observed TB89 values. However, for Le36, sensitivity to CT height is similar to or lower than sensitivity to TB36. Based on these results, we conclude that the acquisition of accurate LWP estimates using TB36 over land requires reduced errors in observed TB36 and radiation from land, as well as a reduced CT height setting.

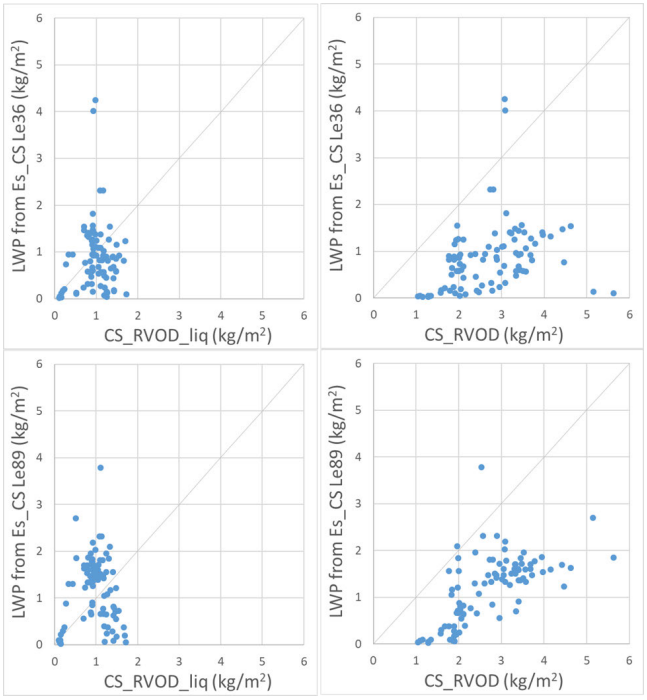

Fig. 15. Scatter plots of LWPs from CloudSat products [(left) CS_RVOD_liq and (right) CS_RVOD] and Es_CS of (top) Le36 and (bottom) Le89.

In summary, an examination of the results from Es_AM and Es_CS using Le36 and Le89 demonstrated that LWP estimation can be performed using TB36 without TB89 even over land. In particular, the result from Le36 shows a highly good agreement with CS_RVOD_liq. This suggests that TB36 is more appropriate for liquid-only estimation of water content. However, the use of TB36 alone requires greater accuracy in observations and background (land) radiation representation compared with the use of TB89. In this study, the land and atmosphere simultaneous estimation allowed for a more accurate representation of land surface radiation, enabling the estimation of LWP over land using TB36. The importance of the CT height settings and the efficacy of adding this setting to the constraints were also supported. In the real-case simulation, it became possible to estimate LWP values of around 1.0 kg/m^2 by incorporating CT height information. Furthermore, a comparison of the results of Le36 and Le89 showed that 89.0-GHz measurements include sufficient ice water particle information, suggesting that liquid and ice water path partitioning can be conducted using the difference between TB36 and TB89 measurements. In the real-case simulations, when CT height was appropriately set, LWP values of around 1.0 kg/m^2 were well estimated. However, considering the results of the synthetic simulation and the accuracy of future CT height information, further validation and improving the method are necessary for the application to clouds with LWP below 1.5 kg/m^2, which contain rain water, including the incorporation of 89 GHz or other observations.

3) Possible Causes of Overestimations: In this section, we examine the factors causing overestimation near Grid45 in Es_CS using the same RTM used for Le36. The inputs to the RTM, including lower boundary conditions and atmospheric profiles, were calculated by the WRF and SiB2 models for Le36 (see the Appendix). The brightness temperature was calculated by RTM after adjustment of the water vapor and

potential temperature—for example, saturating the layers with clouds and adjusting temperature corresponding to the latent heat of cloud condensation—in the same manner used for Le36, according to the selected vertical distribution of CWC.

Fig. 2 shows TB36 and TB89 at the top of the atmosphere over the ocean for various LWP values calculated by the RTM. As indicated in the top figure of Fig. 2, TB36 gradually decreases while maintaining values around 250 K from the point where LWP exceeds 8 kg/m^2; TB36 had maximum values at 3 and 2 kg/m^2 for vertical and horizontal polarizations, respectively, and then, reached 250 K again at approximately 1.8 and 0.7 kg/m^2.

Le36 uses both horizontal and vertical polarizations to calculate the cost function. Ideally, one LWP value should exist for which the brightness temperatures of horizontal and vertical polarizations simultaneously coincide with the observation, allowing appropriate LWP estimation. However, in reality, because of RTM incompleteness, there is no estimation value of LWP at which the observations in both polarizations perfectly coincide. Therefore, in the estimation procedure, the brightness temperature of each polarization does not coincide with the observation; it converges to a value for which the sum of differences from observations in the two polarizations is minimal. Accordingly, for a specific observed brightness temperature, LWP values smaller and larger than the maximum point may have nearly equal cost functions; even at points where the LWP is small, they may erroneously converge to a large value.

Fig. 2 shows that there are two values of LWP with which the cost functions are nearly equal on both sides of the LWP value at the point of maximum TB36. The area around Grid46 is ocean, and the observed TB36 value was about 262 K at vertical polarization and about 257 K at horizontal polarization. When LWP is around 2∼2.5 kg/m^2, TB36 becomes closer to the observed value, but it is found that TB36 of horizontal polarization shows similar values even when LWP is as high as 5 kg/m^2. Thus, the estimated LWP value may have erroneously been determined at a greater value than the maximum value.

Another possible cause is also considered as follows. Grid45 is ocean and very close to the coast in the model, but observations indicate that land and ocean are mixed within the footprint of this grid. The left figure in Fig. 2 is the brightness temperature calculated by the RTM over land. TB36 for horizontal polarization at Grid46 is 257 K for vertical polarization as described above. This temperature is corresponding to about 4 kg/m^2 of LWP over land while about 6 kg/m^2 over ocean according to Fig. 2. Then, the cost function became minimum with a higher value of LWP than the actual value. Therefore, it is indicated that the overestimation near Grid46 is related to inconsistency between the model settings and the mixed signals from clouds over the ocean and land areas within the footprint. The method developed here includes improvements to ensure that observed values containing mixed signals from land and ocean are corrected using a linear sum based on the ratio of land and ocean. In reality, the linear sum of the ratio of land and ocean is not always applicable. For grid points affected by clouds, no correction was applied, thereby avoiding loss of the cloud signal (as described above). Based on these results, we conclude that accurate correction of the observed TB36 in land–ocean mixed footprints is essential for the further improvement of the method.

VI. Conclusions and Considerations

In this study, we examined the feasibility of a method (Le36) to estimate LWP over land using satellite-based microwave brightness temperatures at 36.5 GHz (TB36) without brightness temperatures at higher frequencies. Le36 uses TB36 because it is less affected by ice particles of clouds, leading to higher accuracy of liquid-only estimation than methods that involve higher frequency measurements. However, cloud signals in TB36 are relatively small, thus requiring a more accurate representation of heterogeneous land radiation. Le36 realized this by simultaneously estimating land and atmospheric states, and then dynamically representing land radiation.

First, we examined an LWP estimation method over land using 36.5 GHz based on simulation results from RTMs and a fundamental understanding of microwave radiative transfer properties. In particular, we found that at 36.5 GHz, there is a range of LWP values where two different LWP values correspond to a single Tb measurement. Therefore, increasing the information content by using both polarizations is necessary to enhance the likelihood of converging to the correct LWP value.

Then, we conducted synthetic simulations to investigate the validity, scope of application, and limitations of the method using TB36. The results indicated that the method can be applied to clouds with a wide range of LWP for cloud-only cases and with LWP greater than 1.5 kg/m^2 for cloud-plus-rain cases even over land if the CT setting is appropriately constrained by independent CT information. In cases without supplementary CT information, there is a need to focus on high-CT (>8000 m) clouds. The shape of the vertical distribution of CWC is also a factor contributing to the error in LWP estimation, but its impact is smaller compared to the setting of CT, making it crucial to first ensure the appropriate configuration of CT.

Then, we applied the system to real cases and evaluated its performance by comparing estimation results with the results from Le89, which uses TB89 instead of TB36, and CloudSat products. The evaluations showed the following results.

LWP estimates of Le36 well matched with CS_RVOD_liq on average and with CS_RVOD in horizontal distribution. Le36 consistently estimated reasonable values and horizontal distribution of LWP, even over land, without the use of high-frequency microwaves. The LWP estimation results and the difference between Le36 and Le89 suggested that Le36 reasonably estimated LWP and performed better for liquid-only estimation than Le89. Without CT information (Es_AM), for clouds with small cloud signals, LWP is underestimated and the performance was not particularly good. However, using CT information (Es_CS), the results of estimation for small LWP are much improved, and LWPs about 1.0 kg/m^2 were well estimated in real cases, indicating the effectiveness of the simultaneous estimation method for land and atmosphere.

The results also show that LWP estimation is more sensitive to brightness temperature for TB36 than for TB89, particularly over land. Therefore, LWP estimation using TB36 requires

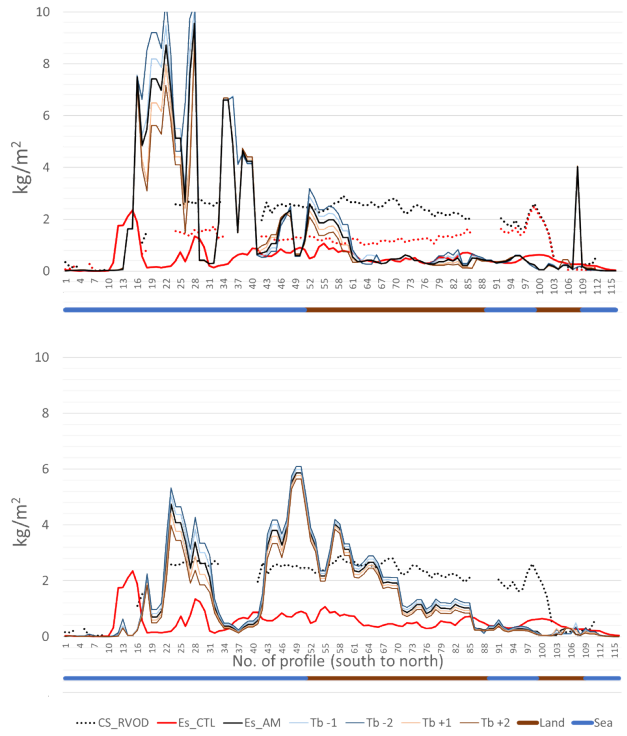

Fig. 16. As described in Fig. 11, but for Case 2.

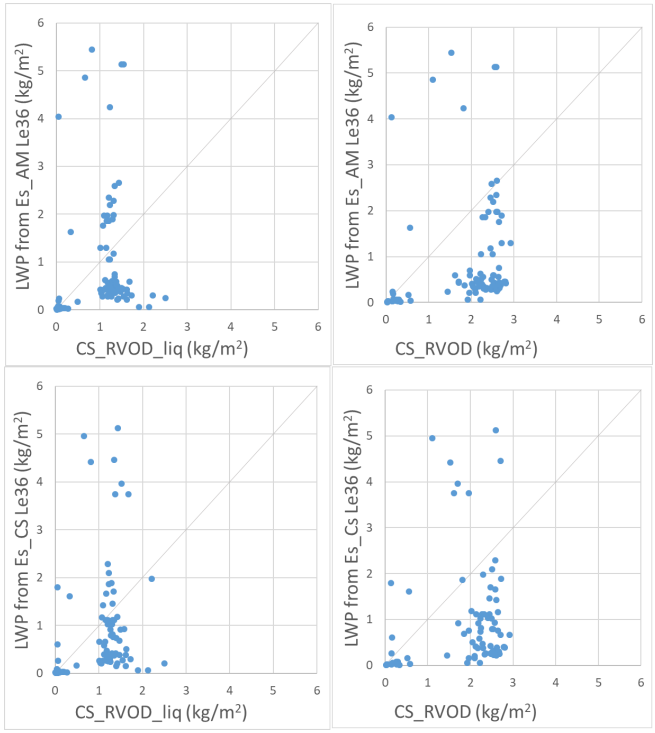

Fig. 17. As described in Fig. 12, but for Case 2.

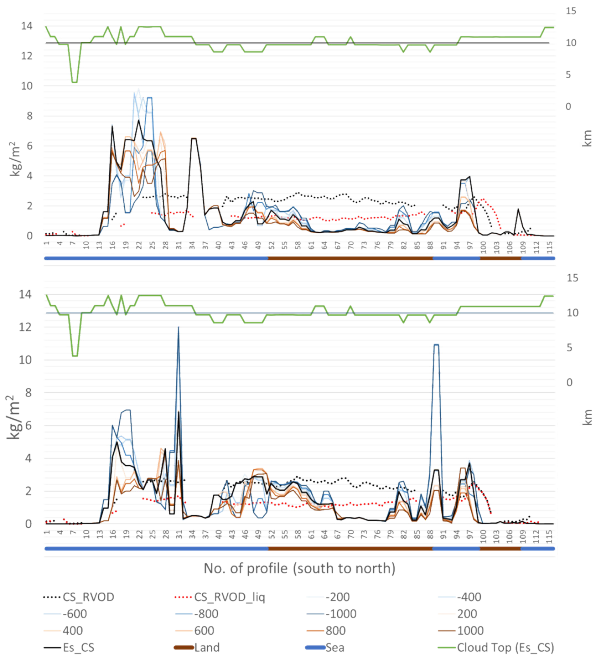

Fig. 18. As described in Fig. 13, but for Case 2.

higher accuracy estimation, including a more appropriate representation of land radiation compared with estimation using TB89. Taking these factors into consideration, the results of real-case simulations indicate the promising performance of Le36 in liquid-only LWP estimation over land. In addition, the method can reduce the information requirements for LWP estimation, conserving high-frequency microwave observations for further partitioning estimation, thereby enabling estimation of the ice cloud water path from the difference between TB36 and TB89. Furthermore, Le89 exhibits a little superior performance in estimating small LWP values. Therefore, it can be inferred that combining TB89 with Le36 would be advantageous for estimating LWP within this range.

Based on our findings from both synthetic and real-case simulations that estimated LWP is highly sensitive to CT height, LWP estimation error can be reduced by improving the setting of CT height. The cloud radar products from CloudSat used to identify the CT height in real-case studies have very narrow spatiotemporal coverage; therefore, information about CT height cannot be directly applied to the estimation of LWP. However, using near-infrared observations and temperature profiles obtained by other satellites with wide coverage and high observation frequency (e.g., Himawari 8), CT height can be estimated. Using these data as boundary conditions for the estimation process should improve LWP estimation accuracy by Le36.

Because 36.5 GHz has a large footprint, numerous observations include both land and ocean areas within a footprint although the corresponding grid is designated as either land or ocean in the model. In such areas, estimated LWP values can become excessive and inconsistent with values in surrounding areas. Therefore, we need to thoroughly investigate the quality check of observation data involving mixed ocean and land areas, as well as the methods for data correction.

As described above, information regarding the distribution of hydrometeor types is essential for comprehension and accurate representation of cloud characteristics; however, such information has been difficult to simultaneously estimate over land and on the basis of satellite data. The findings in this study imply that reasonable LWP (liquid-only cloud and rain water path) estimation can be conducted even over land using satellite passive microwave measurements at 36.5 GHz, without measurements at higher frequencies. In addition, higher frequency measurements include information regarding ice water content. Therefore, in the next step, these measurements

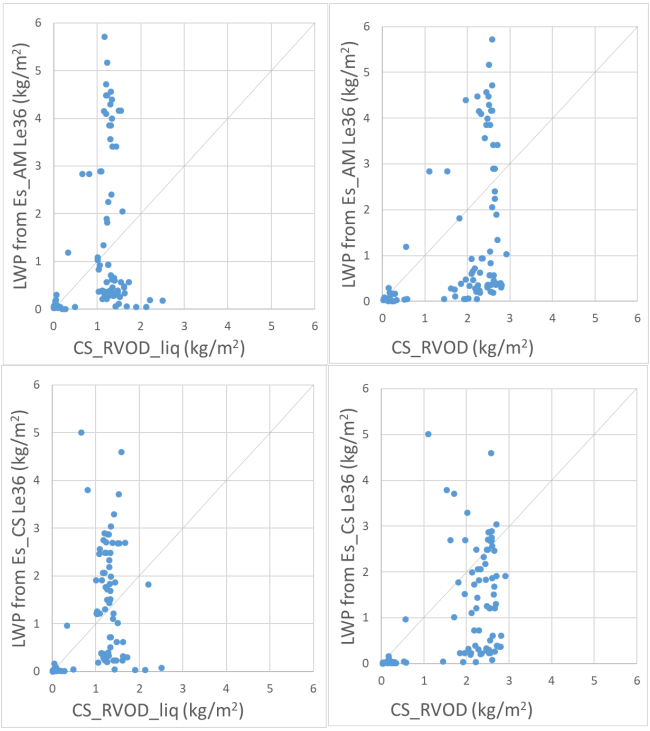

Fig. 19. As described in Fig. 14, but for Case 2.

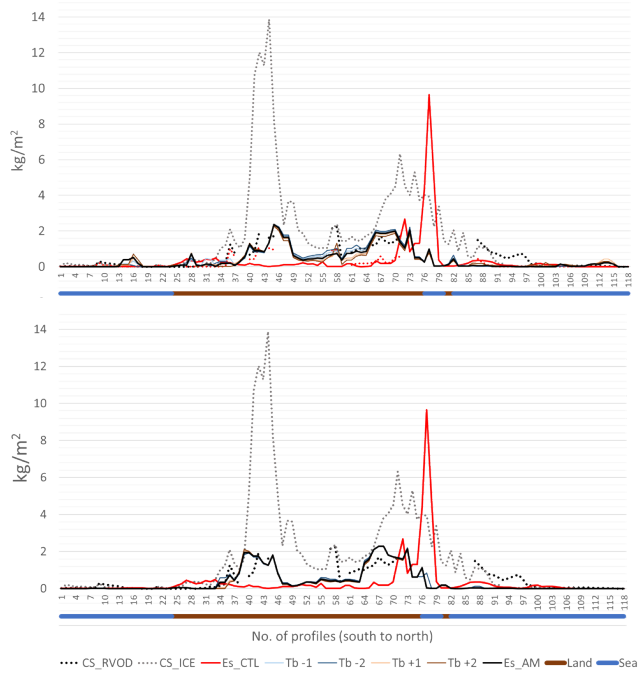

Fig. 20. As described in Fig. 11, but for Case 3.

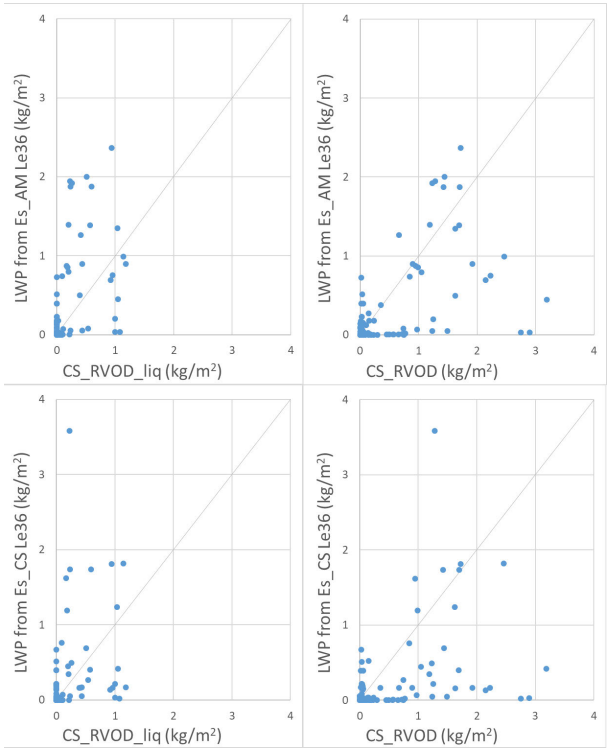

Fig. 21. As described in Fig. 12, but for Case 3.

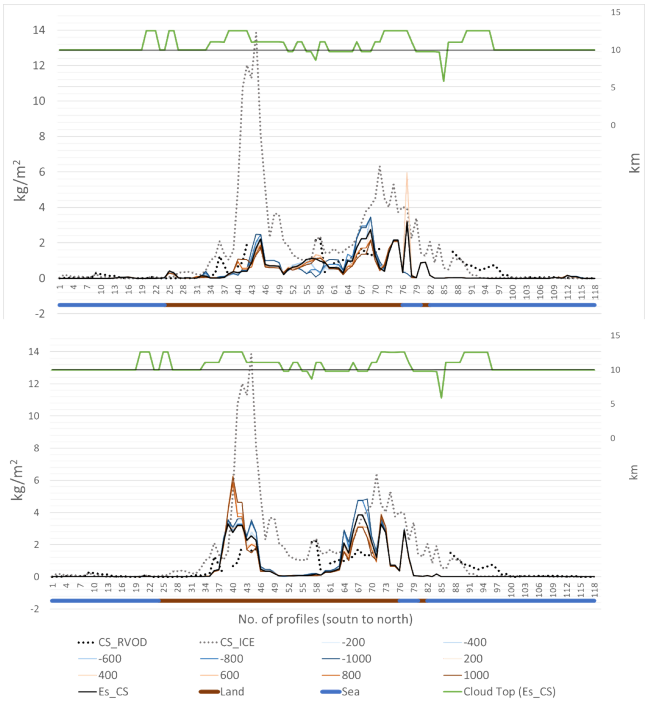

Fig. 22. As described in Fig. 13, but for Case 3.

can be used in the partitioning estimation of liquid and ice water paths.

Furthermore, cloud and rain partitioning estimation using LWP estimates from Le36 is important for future development because the variety of hydrometeors within a cloud system determines the lifetime of the system and its precipitation characteristics, as noted in Section I.O'Dell et al. [10] and Elsaesser et al. [11] reported long-term climatology for cloud LWP and LWP (the sum of cloud and rainwater paths) based on the aggregation of products from several passive microwave retrieval methods. However, because these retrieval methods cannot directly estimate the rainwater path, they constructed data for the LWP using the rainwater path derived from an empirical relationship with rainfall rate. These assumptions related to liquid cloud and rainwater partitioning have been identified as a major source of systematic errors in their results. Lebsock and Su [8] also reported that partitioning of the emission signal between cloud and rainwater is presumably the greatest source of error in the estimation of cloud LWP. The

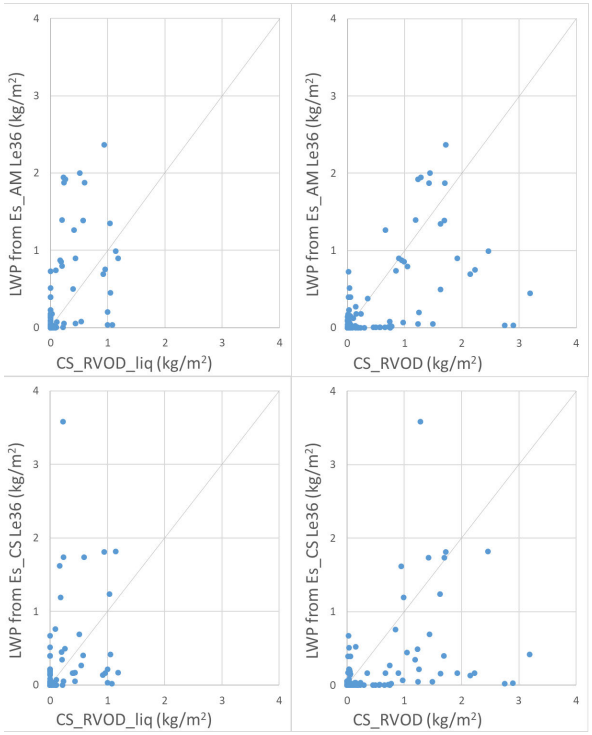

Fig. 23. As described in Fig. 14, but for Case 3.

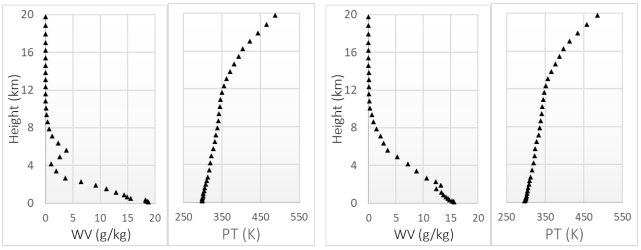

Fig. 24. Examples of water vapor and potential temperature profiles for the RTM simulations shown in Fig. 2. (Left) Over the ocean. (Right) Over land.

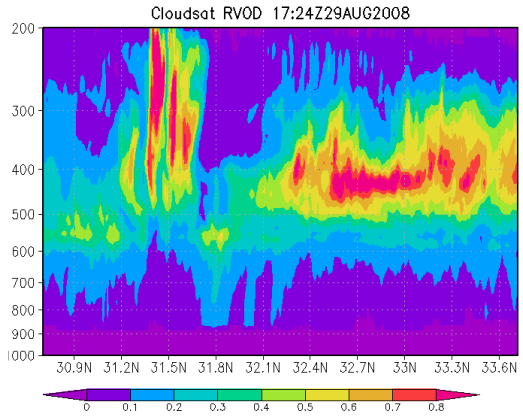

Fig. 25. Vertical profile of CS_RVOD (g/m^3) for Case 1.

scattering effect of rain particles depends on particle oblateness, which can affect the difference between horizontal and vertical polarizations; accordingly, raindrops tend to induce more scatter for horizontally polarized microwaves than for vertically polarized microwaves [39], [40]. For TB36, the difference between polarizations is relatively large. Specifically, the difference in TBs between polarizations at the top of the atmosphere is affected by the extent of hydrometeor attenuation. Cloud and rain particles have attenuation coefficients that are close to a first-order approximation, but at 36.5 GHz, precipitation often has a larger distinction coefficient than clouds. Thus, even with identical radiation from the land surface, the radiation reaching the upper atmosphere will vary depending on the cloud and precipitation composition. Therefore, the polarization difference in radiation observed at the top of the atmosphere—over land and at 36.5 GHz—is a function of the attenuation coefficient, which is smaller when there is additional precipitation than clouds, even when the total amount of moisture in the atmosphere is identical. These considerations support the possibility of an algorithm for separate estimation of cloud and rainwater paths based on the polarization characteristics of TB36 and using Le36-measured LWP as the total LWP. As synthetic simulations showed, one of the reasons for the low estimation accuracy of small LWP clouds is the presence of a mixture of clouds and rain. Thus, there is a possibility that distinguishing between clouds and rain more effectively could improve the estimation of small LWP of rainy clouds.

To enhance the estimation method, it is necessary to explore additional aspects, such as preprocessing and enhancing the quality of observational data, including technical considerations such as optimizing CT height settings. Also, it is imperative to conduct further verification using diverse sources of observations in order to establish a robust and comprehensive method for accurate cloud water path estimation. However, this study has provided the first evidence of the potential to estimate liquid-phase CWC over land using the Ka-band by simultaneously estimating land and atmospheric states and integrating it with CT height information.

APPENDIX

Figs. 16–23 show the results of Cases 2 and 3 corresponding to Figs. 12–15. 2B-CWC-RVOD has fewer missing values compared to 2B-CWC-RO, but it can still exhibit missing values in heavy rainfall areas. Grids near Grid20 and Grid35-40 in Case 2 are likely affected by these missing values. On the other hand, in Le36, CS_RVOD is missing, leading to the overestimation of large LWP values. For Case 3, at many profiles, 2B-CWC-RVOD solid-phase CWC data were missing, so we also used CS_ICE, which is the sum of liquid CWC from 2B-CWC-RVOD and ice CWC from 2C-ICE for reference. The CloudSat products available for comparison are limited, but both Cases 2 and 3 exhibit results similar to Case 1. LWP estimation using Le36 shows a similar averaged value to CS_RVOD_liq (for Case 2: 1.14 and 1.40 kg/m^2 and for Case 3: 0.19 and 0.28 kg/m^2) and well represents the similar 10-km-scale heterogeneity of LWP to CS_RVOD. The sensitivity of estimation on TB36 is greater than that on TB89, and therefore, a more accurate representation of land radiation is required when using TB36. Moreover, although LWP estimates tend to be smaller than those of Le89, as only the liquid-phase CWC signal is captured, the appropriate LWP values are obtained even over land.

Fig. 24 shows atmospheric profile examples used in the RTM simulations shown in Fig. 2. Fig. 25 is the vertical profile of CS_RVOD for Case 1. We determined the cloud layer for LWP estimation in Es_CS based on this profile.

ACKNOWLEDGMENT

This study utilized AMSR-E observed brightness temperature data provided by JAXA and the National Centers for Environmental Prediction Final Operational Global Analysis data retrieved from the National Center for Atmospheric Research (NCAR) website (http://rda.ucar.edu/datasets/ds083.2/). The Radar-AMeDAS data were provided by The Japan Meteorological Agency.

REFERENCES

[1] A. Robert and Houze Jr., *Cloud Dynamics*, vol. 496, 2nd ed. Oxford, U.K.: Academic Press, 2014.

[2] E. Nakakita, H. Sato, R. Nishiwaki, H. Yamabe, and K. Yamaguchi, "Early detection of baby-rain-cell aloft in a severe storm and risk projection for urban flash flood," *Adv. Meteorol.*, vol. 2017, pp. 1–15, Jan. 2017, doi: 10.1155/2017/5962356.

[3] D. D. Turner, "Improved ground-based liquid water path retrievals using a combined infrared and microwave approach," *J. Geophys. Res., Atmos.*, vol. 112, no. 15, Aug. 2007, Art. no. D15204, doi: 10.1029/2007JD008530.

[4] F. J. Wentz, "SSM/I version-7 calibration report," Remote Sensing Syst. (RSS), Santa Rosa, CA, USA, Tech. Rep., 46, 2020. [Online]. Available: http://images.remss.com/papers/tech_reports/2012_Wentz_011012_Version-7_SSMI_Calibration.pdf

[5] K. A. Hilburn and F. J. Wentz, "Intercalibrated passive microwave rain products from the unified microwave ocean retrieval algorithm (UMORA)," *J. Appl. Meteorol. Climatol.*, vol. 47, no. 3, pp. 778–794, Mar. 2008, doi: 10.1175/2007JAMC1635.1.

[6] C. Kummerow, W. S. Olson, and L. Giglio, "A simplified scheme for obtaining precipitation and vertical hydrometeor profiles from passive microwave sensors," *IEEE Trans. Geosci. Remote Sens.*, vol. 34, no. 5, pp. 1213–1232, 1996, doi: 10.1109/36.536538.

[7] T. J. Greenwald, R. Bennartz, M. Lebsock, and J. Teixeira, "An uncertainty data set for passive microwave satellite observations of warm cloud liquid water path," *J. Geophys. Res., Atmos.*, vol. 123, no. 7, pp. 3668–3687, Apr. 2018, doi: 10.1002/2017JD027638.

[8] M. Lebsock and H. Su, "Application of active spaceborne remote sensing for understanding biases between passive cloud water path retrievals," *J. Geophys. Res., Atmos.*, vol. 119, no. 14, pp. 8962–8979, Jul. 2014, doi: 10.1002/2014JD021568.

[9] J. C. Alishouse et al., "Determination of cloud liquid water content using the SSM/I," *IEEE Trans. Geosci. Remote Sens.*, vol. 28, no. 5, pp. 817–822, Sep. 1990, doi: 10.1109/36.58968.

[10] C. W. O'Dell, F. J. Wentz, and R. Bennartz, "Cloud liquid water path from satellite-based passive microwave observations: A new climatology over the global oceans," *J. Climate*, vol. 21, no. 8, pp. 1721–1739, Apr. 2008, doi: 10.1175/2007JCLI1958.1.

[11] G. S. Elsaesser, C. W. O'Dell, M. D. Lebsock, R. Bennartz, T. J. Greenwald, and F. J. Wentz, "The multisensor advanced climatology of liquid water path (MAC-LWP)," *J. Climate*, vol. 30, no. 24, pp. 10193–10210, Dec. 2017, doi: 10.1175/JCLI-D-16-0902.1.

[12] D. I. Duncan, C. D. Kummerow, and W. N. Meier, "An integrated examination of AMSR2 products over ocean," *IEEE J. Sel. Topics Appl. Earth Observ. Remote Sens.*, vol. 10, no. 9, pp. 3963–3974, Sep. 2017, doi: 10.1109/JSTARS.2017.2718535.

[13] M. Kazumori, T. Egawa, and K. Yoshimoto, "A retrieval algorithm of atmospheric water vapor and cloud liquid water for AMSR-E," *Eur. J. Remote Sens.*, vol. 45, no. 1, pp. 63–74, Jan. 2012, doi: 10.5721/EuJRS20124507.

[14] F. J. Wentz and T. Meissner. (2007). *Supplement 1 Algorithm Theoretical Basis Document for AMSR-E Ocean Algorithms. AMSR-E/Aqua L2B Global Swath Ocean Products derived From Wentz Algorithm*. Accessed: Nov. 4, 2020. [Online]. Available: https://nsidc.org/sites/nsidc.org/files/technical-references/amsr_atbd_supp07_ocean.pdf

[15] A. S. Jones and T. H. Vonder Haar, "Passive microwave remote sensing of cloud liquid water over land regions," *J. Geophys. Res., Atmos.*, vol. 95, no. 10, pp. 16673–16683, Sep. 1990, doi: 10.1029/JD095iD10p16673.

[16] R. Seto, T. Koike, and S. Kanae, "Representing cloud water content of extensive cloud systems over land using satellite-based passive microwave observations with a coupled land and atmosphere assimilation method," *J. Geophys. Res., Atmos.*, vol. 123, no. 22, pp. 12829–12856, Nov. 2018, doi: 10.1029/2018JD028864.

[17] F. Ulaby, R. K. Moore, and A. Fung, *Microwave Remote Sensing: Active and Passive, Volume I: Microwave Remote Sensing Fundamentals and Radiometry*, vol. 456. Dedham, MA, USA: Artech House, 1986.

[18] R. F. Adler, R. A. Mack, N. Prasad, I. M. Hakkarinen, and H.-Y.-M. Yeh, "Aircraft microwave observations and simulations of deep convection from 18 to 183 GHz. Part I: Observations," *J. Atmos. Ocean. Technol.*, vol. 7, no. 3, pp. 377–391, Jun. 1990, doi: 10.1175/1520-0426(1990)007<0377:AMOASO>2.0.CO;2.

[19] R. Bennartz and P. Bauer, "Sensitivity of microwave radiances at 85–183 GHz to precipitating ice particles," *Radio Sci.*, vol. 38, no. 4, pp. 1–8, Aug. 2003, doi: 10.1029/2002RS002626.

[20] (2005). *International Telecommunication Union: Specific Attenuation Model for Rain for Use in Prediction Methods*. Accessed: Nov. 4, 2020. [Online]. Available: https://www.itu.int/rec/R-REC-P/en

[21] R. Seto, K. Aida, T. Koike, and S. Kanae, "Radiative characteristics at 89 and 36 GHz for satellite-based cloud water estimation over land," *IEEE Trans. Geosci. Remote Sens.*, vol. 59, no. 2, pp. 1355–1368, Feb. 2021, doi: 10.1109/TGRS.2020.2996239.

[22] G. Liu, "A fast and accurate model for microwave radiance calculations," *J. Meteorological Soc. Jpn. Ser. II*, vol. 76, no. 2, pp. 335–343, 1998, doi: 10.2151/jmsj1965.76.2_335.

[23] R. Seto, T. Koike, and M. Rasmy, "Heavy rainfall prediction applying satellite-based cloud data assimilation over land," *J. Geophys. Res., Atmos.*, vol. 121, no. 16, pp. 9737–9755, Aug. 2016, doi: 10.1002/2016JD025291.

[24] W. C. Skamarock et al., "A description of the advanced research WRF version 3 (no. NCAR/TN-475+STR)," Mesoscale Microscale Meteorol. Division, Nat. Center Atmos. Res., Univ. Corp. Atmospheric Res., Boulder, CO, USA, Tech. Rep. NCAR/TN–475+STR, Jun. 2008, doi: 10.5065/D68S4MVH.

[25] P. J. Sellers et al., "A revised land surface parameterization (SiB2) for atmospheric GCMs, Part I: Model formulation," *J. Climate*, vol. 9, no. 4, pp. 676–705, 1996, doi: 10.1175/1520-0442(1996)009<0676:ARLSPF>2.0.CO;2.

[26] P. J. Sellers et al., "A revised land surface parameterization (SiB2) for atmospheric GCMS. Part II: The generation of global fields of terrestrial biophysical parameters from satellite data," *J. Climate*, vol. 9, no. 4, pp. 706–737, Apr. 1996, doi: 10.1175/1520-0442(1996)009<0706:ARLSPF>2.0.CO;2.

[27] D. N. Kuria, T. Koike, H. Lu, H. Tsutsui, and T. Graf, "Field-supported verification and improvement of a passive microwave surface emission model for rough, bare, and wet soil surfaces by incorporating shadowing effects," *IEEE Trans. Geosci. Remote Sens.*, vol. 45, no. 5, pp. 1207–1216, May 2007, doi: 10.1109/TGRS.2007.894552.

[28] H. Lu, T. Koike, T. Ohta, H. Fujii, and H. Tsutsui, "Improving the AMSR-E soil moisture algorithm of the university of Tokyo through field experiments and parameters optimization," in *Proc. IEEE Int. Geosci. Remote Sens. Symp.*, Feb. 2008, pp. 65–68, doi: 10.1109/IGARSS.2008.4778928.

[29] G. Evensen, "The ensemble Kalman filter: Theoretical formulation and practical implementation," *Ocean Dyn.*, vol. 53, no. 4, pp. 343–367, Nov. 2003, doi: 10.1007/s10236-003-0036-9.

[30] Q. Y. Duan, V. K. Gupta, and S. Sorooshian, "Shuffled complex evolution approach for effective and efficient global minimization," *J. Optim. Theory Appl.*, vol. 76, no. 3, pp. 501–521, Mar. 1993, doi: 10.1007/BF00939380.

[31] M. P. Cadeddu, R. Marchand, E. Orlandi, D. D. Turner, and M. Mech, "Microwave passive ground-based retrievals of cloud and rain liquid water path in drizzling clouds: Challenges and possibilities," *IEEE Trans. Geosci. Remote Sens.*, vol. 55, no. 11, pp. 6468–6481, Nov. 2017, doi: 10.1109/TGRS.2017.2728699.

[32] G. L. Stephens et al., "CloudSat mission: Performance and early science after the first year of operation," *J. Geophys. Res., Atmos.*, vol. 113, no. 8, Apr. 2008, Art. no. DO0A18, doi: 10.1029/2008JD009982.

[33] S. Lee, B. H. Kahn, and J. Teixeira, "Characterization of cloud liquid water content distributions from CloudSat," *J. Geophys. Res., Atmos.*, vol. 115, no. 20, Oct. 2010, Art. no. D20203, doi: 10.1029/2009JD013272.

[34] R. T. Austin, A. J. Heymsfield, and G. L. Stephens, "Retrieval of ice cloud microphysical parameters using the CloudSat millimeter-wave radar and temperature," *J. Geophys. Res., Atmos.*, vol. 114, no. 8, pp. 1–19, Apr. 2009, doi: 10.1029/2008JD010049.

[35] M. Deng, G. G. Mace, Z. Wang, and H. Okamoto, "Tropical composition, cloud and climate coupling experiment validation for cirrus cloud profiling retrieval using CloudSat radar and CALIPSO LiDAR," *J. Geophys. Res., Atmos.*, vol. 115, no. 10, pp. 1–18, May 2010, doi: 10.1029/2009JD013104.

[36] H. Okamoto, K. Sato, and Y. Hagihara, "Global analysis of ice microphysics from CloudSat and CALIPSO: Incorporation of specular reflection in LiDAR signals," *J. Geophys. Res. Atmos.*, vol. 115, no. 22, pp. 1–20, 2010, doi: 10.1029/2009JD013383.

[37] M. Deng, G. G. Mace, Z. Wang, and R. P. Lawson, "Evaluation of several A-Train ice cloud retrieval products with in situ measurements collected during the SPARTICUS campaign," *J. Appl. Meteorol. Climatol.*, vol. 52, no. 4, pp. 1014–1030, Apr. 2013, doi: 10.1175/JAMC-D-12-054.1.

[38] M. Deng, G. G. Mace, Z. Wang, and E. Berry, "CloudSat 2C-ICE product update with a new Ze parameterization in LiDAR-only region," *J. Geophys. Res., Atmos.*, vol. 120, no. 23, pp. 12198–12208, Dec. 2015, doi: 10.1002/2015JD023600.

[39] H. Czekala, and C. Simmer, "Microwave radiative transfer with nonspherical precipitating hydrometeors," *J. Quant. Spectrosc. Radiat. Transf.*, vol. 60, no. 3, pp. 365–374, 1998, doi: 10.1016/S0022-4073(98)00012-0.

[40] H. Czekala, S. Crewell, C. Simmer, and A. Thiele, "Discrimination of cloud and rain liquid water path by groundbased polarized microwave radiometry," *Geophys. Res. Lett.*, vol. 28, no. 2, pp. 267–270, Jan. 2001, doi: 10.1029/2000GL012247.

[41] R. Bennartz and G. W. Petty, "The sensitivity of microwave remote sensing observations of precipitation to ice particle size distributions," *J. Appl. Meteor.*, vol. 40, pp. 345–364, Mar. 2001, doi: 10.1175/1520-0450(2001)040<0345:TSOMRS>2.0.CO;2.

Rie Seto (Member, IEEE) received the B.S., M.S., and Ph.D. degrees from the Department of Civil Engineering, The University of Tokyo, Tokyo, Japan, in 2010, 2012, and 2015, respectively.

From 2017 to 2022, she was an Assistant Professor with the Tokyo Institute of Technology, Tokyo. She is currently a Researcher with the Meteorological Research Institute, Japan Meteorological Agency, Tsukuba. Her research interests include hydrometeorology, remote sensing, and monitoring and prediction of cloud and precipitation over land.

Toshio Koike received the bachelor's, master's, and D.Eng. degrees from The University of Tokyo, Tokyo, Japan, in 1980, 1982, and 1985, respectively.

He was a Research Associate and a Lecturer with The University of Tokyo in 1985 and from 1986 to 1987, respectively, and an Associate Professor and a Professor with the Nagaoka University of Technology, Nagaoka, Japan, from 1988 to 1999 and in 1999, respectively. In 1999, he joined the Department of Civil Engineering, The University of Tokyo, where he was a Professor until 2017. He is currently the Executive Director of the International Centre for Water Hazard and Risk Management (ICHARM), Tsukuba, Japan, under the auspices of the United Nations Educational, Scientific and Cultural Organization (UNESCO) and a Professor Emeritus with The University of Tokyo. His research interests are in hydrology, water resources, satellite remote sensing, climate change, and Asian monsoons.

Dr. Koike has been chairing the River Council of Japan since 2015 and led discussions on important river-related matters to advise the Minister of Land, Infrastructure, Transport and Tourism of Japan.

Misako Kachi received the bachelor's degree in Earth and planetary physics from Hokkaido University, Sapporo, Japan, in 1993, and the M.S. degree in Earth and planetary science from The University of Tokyo, Tokyo, Japan, in 1995.

She joined the National Space Development Agency of Japan [predecessor of Japan Aerospace Exploration Agency (JAXA), Tsukuba, Japan] in 1996. From 2003 to 2005, she was with the Japanese Ministry of Education, Culture, Sports, Science and Technology (MEXT) as a Secretariat Member for the Ad-Hoc Group on Earth Observations and the Earth Observation Summits. In 2005, she joined the Earth Observation Research Center (EORC), JAXA. She currently serves as the Manager of Aqua and Global Change Observation Mission—Water (GCOM-W) and Advanced Microwave Scanning Radiometer 3 (AMSR3) Research and Marine Environment Monitoring at EORC. She is currently a Senior Researcher with EORC, JAXA. Her research interests include microwave remote sensing and its application to other research/operational fields.

Ms. Kachi is a member of the Japan Geophysical Union (JpGU), the Meteorological Society of Japan, and the American Geophysical Union (AGU). She received the Prizes for Science and Technology and the Commendation for MEXT in 2016 [for Global Satellite Mapping of Precipitation (GSMaP)] and 2021 (for Today's Earth).